*Biology of Reproduction*, 2025, **00**, 1–18
https://doi.org/10.1093/biolre/ioaf051
**Research Article**

# Novel insights into human CRISP2: localization in reproductive tissues and sperm, and molecular characterization†

**Thibault Masai[1], Amandine Delnatte[1], Marie Dendievel[1], Denis Nonclercq[2], Annica Frau[2], Jean-François Simon[3], Vanessa Arcolia[3], Ruddy Wattiez[4], Baptiste Leroy[4], Patricia S. Cuasnicu[5], Pascale Lybaert[6] and Elise Hennebert[1,*]**

[1]Laboratory of Cell Biology, Research Institute for Biosciences, Research Institute for Health Sciences and Technology, University of Mons, Mons, Belgium
[2]Laboratory of Histology, Research Institute for Health Sciences and Technology, University of Mons, Mons, Belgium
[3]Clinique de Fertilité Régionale de Mons, Centres Hospitaliers Universitaires (CHU) HELORA—Hôpital de Mons site Kennedy, Mons, Belgium
[4]Laboratory of Proteomics and Microbiology, Research Institute for Biosciences, University of Mons, Mons, Belgium
[5]Instituto de Biología y Medicina Experimental - Consejo Nacional de Investigaciones Científicas y Técnicas (IByME-CONICET), Ciudad Autónoma de Buenos Aires, Argentina
[6]Research Laboratory on Human Reproduction, Faculty of Medicine, Université libre de Bruxelles, Brussels, Belgium

*__Correspondence:__ Laboratory of Cell Biology, Research Institute for Biosciences, Research Institute for Health Sciences and Technology, University of Mons, Place du Parc 23, 7000 Mons, Belgium. E-mail: elise.hennebert@umons.ac.be

†__Grant Support:__ This work was funded by UMons Research Institute for Biosciences, by the Fund for Scientific Research of Belgium (F.R.S.—FNRS) under Grant Equipment UN07220F, by the Programme Wallon d'investissement: Région Wallonne—UMONS n°1910169 dans le domaine de INSTIMAG (Instruments d'imagerie) for the acquisition of the Nikon TI2-E-A1RHD25 confocal microscope, and by the European Regional Development Fund and the Walloon Region as part of support for the Bioprofiling platform, Belgium. TM is a FRIA grantee of the F.R.S.—FNRS.

## Abstract

CRISP2 is enriched in the male reproductive system of mammals and plays roles in spermatogenesis, sperm motility, and fertilization. Although extensively investigated in rodents and boars, human CRISP2 (hCRISP2) remains poorly studied, particularly concerning its localization in testicular and epididymal tissues and its molecular features. In this study, we used immunofluorescence to determine the localization of hCRISP2 in testis, epididymis, and ejaculated sperm. While no expression was observed in the epididymal epithelium, hCRISP2 was detected at different stages during spermatogenesis. Specifically, hCRISP2 was found in the nucleus of primary spermatocytes and of both round and early elongated spermatids. In elongated spermatids, it was additionally observed in the cytoplasm, the flagellum, and the equatorial segment of the acrosome (EqS). The presence of aggregated material with hCRISP2 immunoreactivity in the apical pole of Sertoli cells suggests that most of the hCRISP2 involved in spermatogenesis is phagocytized by these cells during spermiation. In ejaculated sperm, hCRISP2 was found in the cytoplasmic droplet, flagellum, and EqS, consistent with its described roles in sperm motility and gamete fusion. Native and denaturing electrophoresis combined with western blot analyses depicted the ability of hCRISP2 to form stable high molecular weight complexes, and mass spectrometry revealed that these complexes likely consist exclusively of hCRISP2. Furthermore, we showed that hCRISP2 undergoes only limited post-translational modifications. These findings shed light into the dynamic localization of hCRISP2 throughout spermatogenesis and in ejaculated sperm, as well as its molecular features, enhancing our understanding of its functional roles and relevance for male fertility.

**Summary Sentence**
hCRISP2 is present at different stages of spermatogenesis, absent in epididymal epithelium, and, in mature sperm, localizes in the cytoplasmic droplet, flagellum, and EqS, forming stable homo-oligomers with minimal post-translational modifications.

**Received:** July 15, 2024. **Revised:** November 20, 2024. **Accepted:** March 11, 2025

## Graphical Abstract

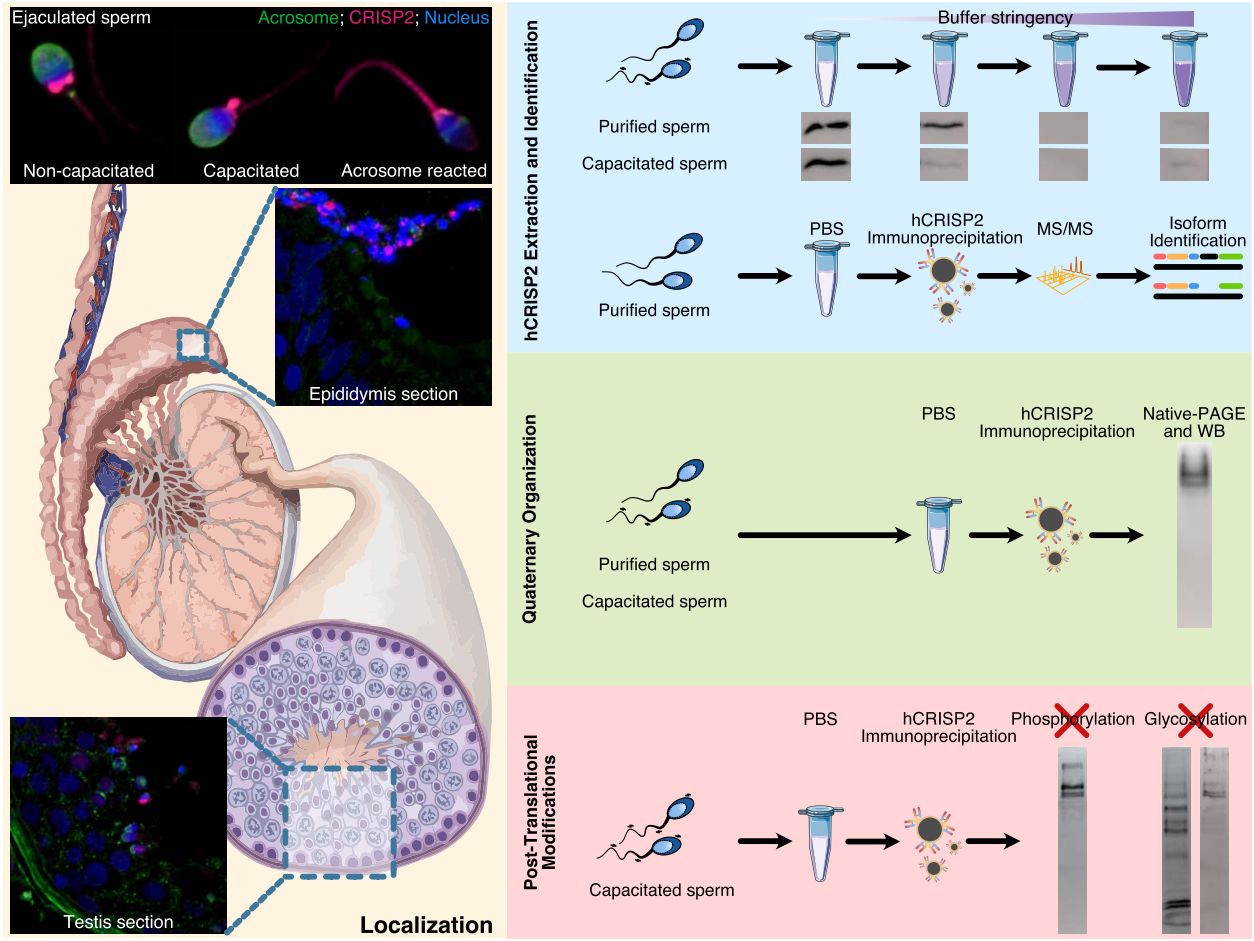


**Key words:** hCRISP2, human, spermatogenesis, epididymis, sperm, immunofluorescence, protein characterization, oligomers.

## Introduction

The cysteine-rich secretory proteins (CRISPs) belong to a super-family of proteins named "Cysteine-rich secretory proteins, Antigen 5, and Pathogenesis-related 1" (CAP) [1, 2]. CRISPs are only expressed in vertebrates and, in mammals, are enriched in the male reproductive system [3]. Indeed, evidence showed that mammalian CRISPs play key roles in the fertilization process as recently reviewed [4]. Eight intramolecular disulfide bonds stiffen and shape these proteins [5, 6] which are composed of two evolutionary conserved and structured domains linked by a hinge region [6]: an N-terminal CAP domain with a proposed cell–cell interaction function [7, 8] and a C-terminal cysteine-rich domain with ion channel regulatory activity [9].

Most studies on CRISPs have been carried out in mice and rats, in which four (mCRISP1, 2, 3, and 4) and three (rCRISP1, 2, and 4) proteins have been described, respectively [10]. In humans, the expression of three CRISPs has been reported (hCRISP1, 2, and 3) [2]. Based on sequence homology, tissue distribution, and in vitro experiments, hCRISP1 has been shown to serve as the functional equivalent of the combination of rodent CRISP1 and 4 [11–13]. The expression of CRISP1, CRISP3, and CRISP4 has been shown to be androgen regulated in different species [11, 14–20]. In rodents and humans, these proteins are produced and secreted by the epididymal epithelium [5, 11, 12, 21, 22] and associate with the surface of sperm during their journey within the male genital tract [22–24]. Additionally, CRISP3 is also expressed in the blood in humans [25] and in various secretory organs such as the pancreas, salivary glands, prostate, and vas deferens ampulla, depending on the species [2, 14, 20, 22, 26]. Unlike the other CRISPs, CRISP2 is a testicular protein expressed during spermatogenesis in an androgen-independent manner. The exact stage at which the protein is expressed varies in the literature depending on the species and even on the study within the same species (Supplementary Table 1) [27–31].

CRISP2 is a versatile protein for which multiple functions have been described in different species: (1) it was found to interact with Sertoli cells during spermatogenesis in rats [27], (2) it regulates sperm motility and acrosome reaction (AR) in mice [9, 32, 33], and (3) it mediates the interaction with the oocyte during gamete fusion in humans and mice [34, 35]. These different functions involve the presence of CRISP2 both within sperm and on its surface. However, a literature survey reveals that investigating the localization of CRISP2 is not straightforward. CRISP2 localization in sperm has been studied in rodents [28, 35–41], humans [34, 42, 43], boars

[31, 44, 45], wild cats [46], and Malayan tapirs [47]. While it is almost systematically detected in the connecting piece (or neck), it is also described at other localizations (acrosome, perinuclear theca (PT), and/or flagellum), depending on the study (Supplementary Table 1, see also Supplementary Figure 1 for illustration of sperm-specific regions referred to in this paper). In humans and mice, acrosomal CRISP2 has been shown to relocalize to the equatorial segment of the acrosome (EqS) after the AR [34, 35]. Subsequently, in humans, it was demonstrated that it actually reassociates with the plasma membrane covering this region, implicating CRISP2 in gamete fusion, as the EqS is the region through which sperm fuses with the plasma membrane of the oocyte [42]. Recently, different results obtained in boars suggested that CRISP2 is present in the PT rather than in the acrosome [44, 45, 48]. For this species, capacitation results in relocalization of CRISP2 to the apical end of the head, as well as to the EqS. After the AR, only a subdomain of the EqS region remains labeled, presumably still the PT [45].

The molecular characterization of native CRISP2 is still relatively limited in the literature. In studies involving mice, boars, and humans, CRISP2 has consistently been reported as a 25-kDa protein based on sodium dodecyl sulfate–polyacrylamide gel electrophoresis (SDS-PAGE) analysis [34, 35, 42, 44]. However, in rats, CRISP2 appears as two distinct bands of 27 and 25 kDa which are thought to represent CRISP2 with and without its signal peptide, respectively [28, 49]. While CRISP1, 3, and 4 are known to be glycosylated [11, 22, 50–52], only one study has specifically examined the glycosylation status of CRISP2. In that study conducted in guinea pigs, carbohydrate analysis using gas–liquid chromatography did not reveal any sugar residue on CRISP2 [41]. To the best of our knowledge, there is currently no information available regarding other potential post-translational modifications in CRISP2. Interestingly, recent observations in boars showed that CRISP2 from the PT and the flagellum forms stabilized oligomers of different biochemical properties [44].

The aim of the present study is to contribute to the characterization of hCRISP2, which has been less studied compared to CRISP2 from other species. We investigated its localization during spermatogenesis and epididymal maturation as well as in ejaculated sperm before and after capacitation, and following AR. Indeed, given the challenges associated with obtaining human tissue samples, only two studies addressed the localization of hCRISP2 in testis sections [29, 30], and none has examined its presence in the epididymis. Furthermore, although several studies have investigated hCRISP2 localization in sperm, no consensus has been reached, as the results varied among studies [29, 30, 34, 42, 43, 46, 47] (Supplementary Table 1), presumably due to the methods of sample preparation and the use of different antibodies. Here, we used the same set of antibodies raised against hCRISP2, for which we previously validated the specificity, across all our investigations. In addition, we performed experiments to contribute to the molecular characterization of hCRISP2, focusing on its primary and quaternary structures and exploring its post-translational modifications. Overall, we show that hCRISP2 is translated from the primary spermatocyte stage during spermatogenesis and, in mature sperm, is localized in the cytoplasmic droplet, the flagellum, and within the EqS. In mature sperm, hCRISP2 forms stable homo-oligomers with minimal post-translational modifications.

## Materials and methods

### Samples and ethics

Human semen samples were obtained from the fertility clinic of HELORA Hospital (Mons, Belgium) from patients undergoing routine semen analysis or from voluntary donors. All experiments conducted in this study were approved by the Ethics Committee of HELORA Hospital in Mons and by the Ethics Committee of Erasme Hospital in Brussels (EudraCT/CCB:/B4062020000093). The samples were obtained with the informed written consent from all subjects. Semen samples were collected by masturbation after an abstinence period of 3–5 days and routine semen analysis was performed according to the World Health Organization (WHO) 2021 guidelines [53]. Only normozoospermic samples (volume $\geq$1.4 mL, sperm concentration $\geq 16 \times 10^6$/mL, and total motility $\geq$42%) were investigated.

Regarding human testis and epididymis sections, the material was obtained from Erasme Hospital biobank (BE_BERA1; Biobanque Hôpital Erasme-Université Libre de Bruxelles (BERA); Biobanking and Biomolecular Resources Research Infrastructure – European Research Infrastructure Consortium (BBMRI-ERIC)). The sections were taken from tissues sampled at a distance from a malignant region and presenting a normal histology (i.e., complete spermatogenesis in the case of testes).

### Sperm preparation

Sperm purification from the semen samples was carried out by centrifugation at 300×*g* for 20 min at 37°C on a discontinuous PureSperm 40/80 density gradient (Nidacon, Mölndal, Sweden) as described in Nicholson [54] and the WHO guidelines [53]. Purified sperm recovered from the bottom of the 80% PureSperm fraction were then washed with Dulbecco phosphate-buffered saline (Sigma-Aldrich, St Louis, MO, USA) supplemented with 100 $\mu$g/mL ampicillin (Thermo Fisher Scientific, Geel, Belgium).

### In vitro capacitation

Sperm ($1.0 \times 10^7$ cells/mL) were incubated for 4 h at 37°C in an incubator containing 5% $CO_2$ in a capacitation solution composed of homemade Earle's balanced salt solution (116.36 mM sodium chloride, 26.19 mM sodium bicarbonate, 1.01 mM sodium dihydrogen phosphate monohydrate, 5.37 mM potassium chloride, 0.81 mM magnesium sulfate heptahydrate, 5.55 mM D-glucose, 1.80 mM calcium chloride) [53] supplemented with 26 mg/mL of delipidated bovine serum albumin (Fraction V) (Sigma-Aldrich, St Louis, MO, USA), 2.73 mM sodium pyruvate (Carl Roth GmbH, Karlsruhe, Germany), 24.90 mM sodium D, L-lactic acid (Sigma-Aldrich, St Louis, MO, USA), and 100 $\mu$g/mL ampicillin. Sperm were resuspended every hour by gentle agitation. Non-capacitated sperm were incubated for only 3 min under the same conditions.

### Acrosome reaction induction

Capacitated sperm were exposed to 20 $\mu$M calcium ionophore A23187 (Sigma-Aldrich, St Louis, MO, USA) or 50 $\mu$M progesterone (Sigma-Aldrich, St Louis, MO, USA) to induce acrosome reaction. Briefly, inducers (resuspended in dimethyl sulfoxide; Thermo Fisher Scientific) were added to the sperm suspension at the appropriate concentration and sperm were incubated for 1 h at 37°C in an incubator containing 5% $CO_2$.

## Analysis of hCRISP2 localization on ejaculated sperm

Aliquots of sperm from non-capacitated, capacitated, and acrosome-reacted conditions were fixed in an equal volume of 4% (w/v) paraformaldehyde (PAF; Sigma-Aldrich, Burlington, MA, USA) in phosphate-buffered saline (PBS; 137 mM NaCl, 2.7 mM KCl, 10 mM $Na_2HPO_4$, 1.76 mM $KH_2PO_4$, pH 7.4) for 20 min at room temperature. The samples were then centrifuged at 2 000×*g* for 5 min at 4°C. They were washed twice with PBS supplemented with 50 mM glycine, to quench the remaining PAF, and once with PBS. Droplets of 0.1 to $0.2 \times 10^6$ fixed sperm were air dried on 12-mm-diameter glass coverslips. After a quick wash with PBS supplemented with 0.05% (v/v) Tween-20 (Tw; Thermo Fisher Scientific, Waltham, MA, USA), sperm were permeabilized in PBS-Tw containing 0.3% (v/v) Triton X-100 (Carl Roth GmbH, Karlsruhe, Germany) for 20 min. The coverslips were then washed three times for 5 min with PBS-Tw before blocking in PBS-Tw supplemented with bovine serum albumin (BSA; 3% (w/v)) (Carl Roth GmbH, Karlsruhe, Germany) for 45 min at room temperature. Sperm were incubated overnight at 4°C with rabbit polyclonal anti-hCRISP2 (Proteintech, Manchester, UK; Cat# 19066-1-AP) diluted 1:100 in PBS-Tw-BSA (3%). Controls were performed by incubating coverslips in PBS-Tw-BSA (3%) without primary antibody. Following several washes with PBS-Tw, the coverslips were incubated for 1 h at room temperature with Alexa fluor 568–coupled goat anti-rabbit immunoglobulins (Invitrogen, Eugene, OR, USA; Cat# A-11011) diluted 1:100 in PBS-Tw-BSA (3%). After washing with PBS-Tw, acrosome labeling was performed for 30 min at room temperature with a 5 $\mu$g/mL solution of fluorescein isothiocyanate (FITC) conjugated *Pisum sativum* agglutinin (PSA-FITC; Sigma-Aldrich, Burlington, MA, USA; Cat# L0770) diluted in PBS. Finally, the coverslips were washed again with PBS and then mounted on glass slides with Prolong Gold Antifade Mountant with DAPI (Invitrogen, Waltham, MA, USA; Cat# P36941). Z-Stack images of 0.15-$\mu$m increment were collected using a confocal microscope Nikon TI2-E-A1RHD25.

## Analysis of hCRISP2 localization on human testis and epididymis sections

Testis and epididymis sections (5 $\mu$m in thickness) were dewaxed and rehydrated. For each tissue, one section was stained using Masson Trichrome and the others were subjected to an indirect immuno-labeling method according to the following protocol. First, a heat-induced epitope retrieval (HIER) was performed with sodium citrate buffer (21.8 mM citric acid, pH = 6.2). Sections were washed with PBS before blocking in PBS-BSA (5%). Then, hCRISP2 and sperm acrosomes were labeled using the protocol described for ejaculated sperm. Sections were counterstained for 15 min with 10 $\mu$g/mL of Hoechst 33342 (Sigma-Aldrich, St Louis, MO, USA) and mounted with Vectashield Plus (Vector Laboratories, Burlingame, CA, USA). Double immuno-labeling for hCRISP2 and vimentin (used to identify Sertoli cells) was performed using the same protocol but with serial incubations with (1) mouse monoclonal anti-Vimentin (Proteintech, Manchester, UK; Cat# 60330-1-Ig) diluted 1:500 in PBS-BSA (3%) for 2 h at room temperature, (2) rabbit polyclonal anti-hCRISP2 overnight at 4°C, (3) Alexa fluor 568–coupled goat anti-rabbit immunoglobulins for 1 h at room temperature, and (4) CoraLite488 conjugated Affinipure Goat Anti-Mouse (Proteintech, Manchester, UK; Cat# SA00013-1) diluted 1:100 in PBS-BSA (3%) for 1 h at room temperature. Z-Stack images were collected as described for ejaculated sperm, but with 0.1-$\mu$m increment.

## Sperm protein extraction

Aliquots of purified sperm and capacitated sperm were used for protein extractions. Purified sperm were either extracted directly or were flash frozen in liquid nitrogen and stored at −80°C until use. Capacitated sperm were centrifuged at 2 000×*g* for 5 min at 4°C, washed three times with cold PBS, flash frozen in liquid nitrogen, and stored at −80°C until use.

(1) *Denaturing extraction*

Sperm aliquots were incubated for 5 min at room temperature in Laemmli SDS sample buffer (50 mM Tris, 10% (v/v) glycerol, 2% (w/v) sodium dodecyl sulfate (SDS), 100 mM dithiothreitol (DTT; Molekula, Darlington, UK), and bromophenol blue, pH 6.8).

(2) *Native extraction*

Sperm aliquots were vortexed three times for 10 s in PBS supplemented with protease inhibitors (Complete ULTRA Tablets; Roche, Mannheim, Germany) and phosphatase inhibitors (PhosSTOP; Roche, Mannheim, Germany) supplemented or not with 1% Triton X-100. Some samples were submitted to a mechanical lysis using an ultrasound probe (IKA U50 sonicator; Staufen, Germany). Three cycles of sonication of 5 s at 20% amplitude were performed at 4°C. All the samples were incubated for 1 h on ice and then centrifuged at 17 000×*g* for 20 min at 4°C. The resulting supernatant was either directly processed for electrophoresis (see below) or first exposed for 1 h at room temperature to different dissociation agents: (1) 1 M sodium chloride (NaCl, (2) 100 mM DTT, (3) 24 mM ethylenediaminetetraacetate (EDTA), (4) 1% Triton X-100, or (5) 4 M urea.

(3) *Successive extraction*

Sperm aliquots were rapidly thawed, and proteins were successively extracted with (1) PBS, (2) PBS supplemented with 1% Triton X-100 (PBS-T), (3) PBS-T supplemented with 0.5% sodium deoxycholate (PBS-T-D), and (4) Laemmli SDS sample buffer. For each extraction, samples were vortexed three times for 10 s and incubated for 20 min on ice, then centrifuged at 17 000×*g* for 20 min at 4°C. The supernatant collected after each extraction and centrifugation was used for western blot analysis, as described below. Between each extraction, the pellet was washed with PBS to minimize protein transfer from one extraction to the next. All buffers were supplemented with protease inhibitors and phosphatase inhibitors as described for native extraction.

## Human CRISP2 immunoprecipitation

Dynabeads Protein G (Thermo Fisher Scientific, Vilnius, Lithuania) were prepared according to manufacturer guidelines. Briefly, per reaction, 3 $\mu$g of rabbit polyclonal anti-hCRISP2 (Proteintech, Manchester, UK; Cat# 19066-1-AP) were incubated with 50 $\mu$L of Dynabeads. The antibody was crosslinked to the beads using 1 mM bis (sulfosuccinimidyl)

suberate (BS3; Abcam, Amsterdam, Netherlands). Sperm aliquots were extracted in PBS followed by sonication as explained above. After centrifugation at 17 000×*g* for 20 min at 4°C, the supernatant (corresponding to 1 to $4.5 \times 10^7$ sperm) was added to the beads and incubated overnight at 4°C on a rotating shaker. The next day, the beads were washed three times with PBS and resuspended in 50 $\mu$L of 50 mM glycine (pH = 2.8) under vigorous agitation for 10 min at room temperature. The eluate was transferred into a new tube and the acidic pH was promptly neutralized with 5 $\mu$L of 1 M Tris (pH = 7.5). A second elution was carried out under the same condition, neutralized, and pooled with the first one.

## Western blot

(1) *Protein separation by SDS-PAGE*

Sperm protein extracts obtained in Laemmli SDS sample buffer or immunoprecipitated hCRISP2 mixed with Laemmli SDS sample buffer were heated for 5 min at 95°C, centrifuged, and loaded on 12% SDS-PAGE gels. Electrophoresis was carried out with TGS buffer (25 mM Tris, 192 mM glycine, 0.1% (w/v) SDS).

(2) *Protein separation by Native-PAGE*

Sperm protein extracts obtained in PBS or immunoprecipitated hCRISP2 were mixed with native-sample buffer (50 mM Tris, 10% (v/v) glycerol, bromophenol blue, pH = 6.8) supplemented or not with 100 mM DTT, centrifuged, and loaded on 10% Native-PAGE gels. Electrophoresis was carried out for 2 h at 150 V and 4°C with cold TG buffer (25 mM Tris, 192 mM glycine).

(3) *Protein transfer and detection*

After electrophoresis, proteins were transferred onto PVDF membranes (GE Healthcare) using 25 mM Tris, 192 mM glycine, 0.05% (w/v) SDS, and 20% (v/v) methanol as transfer buffer. The membranes were washed with PBS-Tw and then blocked for 1 h in PBS-Tw-BSA (5%). After that, they were incubated overnight at 4°C under gentle agitation with the following antibodies diluted in PBS-Tw-BSA (3%): (1) mouse monoclonal anti-hCRISP2 (D-10) (Santa Cruz Biotechnology, Inc., Heidelberg, Germany; Cat# sc-390,914) (1:1000), (2) rabbit polyclonal anti-hCRISP2 (Proteintech, Manchester, UK; Cat# 19066-1-AP) (1:1 000), (3) mouse monoclonal anti-phosphotyrosine clone 4G10 (Merck KGaA, Darmstadt, Germany; Cat# 05-321X) (1:20 000), or with the following biotinylated lectins diluted in Tris-buffered saline (TBS)-Tw-BSA (3%): (1) peanut agglutinin (PNA) (Vector Laboratories, Burlingame, CA, USA; Cat# 30272) (1:1 000) to detect O-glycosylations or (2) wheat germ agglutinin (WGA) (Vector Laboratories, Burlingame, CA, USA; Cat# 30268) (1:1 000) to detect N-glycosylations. From this point, all buffers were supplemented with 0.1 mM $CaCl_2$ for PNA, and 0.1 mM $CaCl_2$ and 0.01 mM $MnCl_2$ for WGA. After five washes of 5 min in PBS-Tw or TBS-Tw, the membranes were incubated for 1 h at room temperature under gentle agitation with (1) HRP-conjugated goat anti-mouse immunoglobulins (Invitrogen, Eugene, OR, USA; Cat# G-21040) (1:50 000), (2) HRP-conjugated goat anti-rabbit immunoglobulins (Proteintech, Manchester, UK; Cat# SA00001-2) (1:5 000), diluted in PBS-Tw-BSA (3%), or (3) HRP-conjugated streptavidin (Dako, Glostrup, Denmark; Cat# P0397) (1:5 000) diluted in TBS-Tw-BSA (3%). Finally, the membranes were washed again and immunoreactive bands were visualized using the ECL Western Blotting Substrate (Thermo Fisher Scientific, Waltham, MA, USA) and the Fusion FX imaging system (Vilber, Marne-la-Vallée, France).

## Mass spectrometry analyses

Human CRISP2 was immunoprecipitated from frozen purified sperm as described above. Control reactions were performed using: (1) Dynabeads not coupled to any antibody, (2) Dynabeads coupled to a rabbit polyclonal anti-HSP70 (Proteintech, Manchester, UK; Cat# 10995-1-AP), and (3) Dynabeads coupled to rabbit IgG (Proteintech, Manchester, UK; Cat# 30000-0-AP). The eluates were mixed with 10 mM dithioerythritol (DTE; Thermo Fisher Scientific, Geel, Belgium) and incubated for 20 min at 56°C. Then, iodoacetamide (23 mM final concentration; VWR International, Leuven, Belgium) was added and the mixture was incubated in the dark for 30 min at room temperature. The proteins contained in the samples were precipitated overnight at −20°C in cold acetone 80% (v/v). After centrifugation at 21 000×*g* for 20 min at 4°C, the resulting pellet was resuspended in 20 $\mu$L of 5 ng/$\mu$L porcine sequencing grade modified trypsin (Promega, Madison, WI, USA) in 25 mM ammonium bicarbonate ($NH_4HCO_3$; Sigma-Aldrich, St Louis, MO, USA) and incubated overnight at 37°C. Trypsinolysis was terminated with formic acid (0.1% (v/v) final concentration). The resulting peptides were analyzed by reverse-phase HPLC-ESI-MS/MS on a UHPLC-HRMS/MS instrument (AB SCIEX LC420 and TripleTOFTM 6600) using data-dependent acquisition (DDA) mode. Tryptic peptides were separated on a C18 column (YMC-Triat 0.3 mm × 150 mm column) with a linear acetonitrile gradient (5% to 35% of acetonitrile, 5 $\mu$L/min, 75 min) in water containing 0.1% formic acid. The MS survey scans (m/z 400–1250, 100-ms accumulation time, mass resolution of 25 000) were followed by 50 MS/MS acquisition overlapping windows covering the precursor m/z range. Collision-induced dissociation was carried on using rolling collision energy, and fragment ions were accumulated for 50 ms in high sensitivity mode (mass resolution of 10 000). The MS/MS data were processed with ProteinPilot software (version 5.0.1.04895; AB SCIEX) and analyzed against UniProt *Homo sapiens* database with the relevant parameters, including carbamidomethyl cysteine, oxidized methionine, all biological modifications, amino acid substitutions, and missed cleavage site.

## Discrimination between hCRISP2 isoforms

Transcript sequences for hCRISP2 were retrieved from Ensembl (release 111—January 2024) [55] and used to identify exon boundaries. Protein sequences of the two known hCRISP2 isoforms (P16562-1 and P16562-2) were retrieved from UniProt (release 2024_01) [56] and aligned with MUSCLE in Geneious Prime 2023.2.1 (Geneious, Boston, MA, USA). Human CRISP2 peptides were searched in a sperm proteome available in our laboratory and obtained through a DDA proteomic analysis performed on proteins extracted from sperm in different conditions using a TripleTof 6600 mass spectrometer (Sciex, Framingham, MA, USA). Additionally, hCRISP2 peptides were also retrieved from

MS/MS results from immunoprecipitated hCRISP2 obtained as described above. Peptides identified with high confidence and highest-quality MS/MS spectra were selected and were mapped on hCRISP2 isoform alignment.

## Results

### Localization of hCRISP2 in testis and epididymis

To investigate the temporal dynamics of hCRISP2 localization across spermatogenesis, we analyzed its localization on testis sections using immunofluorescence (IF). First, due to the observed variability in CRISP2 immunolocalization across species and studies (Supplementary Table 1), which could, among other causes, be attributed to antibody specificity, we assessed the ability of two different anti-hCRISP2 (i.e., a mouse monoclonal antibody and a rabbit polyclonal antibody) to specifically detect hCRISP2. Both antibodies were able to detect hCRISP2 in human sperm protein extracts by western blot (WB) following SDS-PAGE (Supplementary Figure 2A) while only the polyclonal antibody was able to detect hCRISP2 under native conditions (i.e., Native-PAGE; Supplementary Figure 2B). In addition, both antibodies detected hCRISP2 by immunofluorescence in HeLa cells transfected with an expression vector encoding hCRISP2 but did not label HeLa cells expressing hCRISP1, demonstrating their specificity (Supplementary Figure 2C). Based on these results, the polyclonal antibody was selected to investigate hCRISP2 localization on testis sections by IF. In these experiments, counter-labeling with PSA was used to visualize sperm acrosomes and identify the germ cell stage during spermiogenesis, while anti-vimentin was used to highlight Sertoli cells. An increasing gradient of hCRISP2 immunostaining intensity was observed from the basal compartment to the luminal compartment of the seminiferous tubules, reflecting the progression of hCRISP2 expression during spermatogenesis (Figure 1A, Supplementary Figure 3). For each cell type, equatorial views and 3D reconstructions from confocal z-stacks are provided to accurately illustrate the precise localization of the labeling. Additionally, Masson Trichrome–stained images are included to highlight cellular histology, clearly differentiating between the nucleus and cytoplasm. No hCRISP2 immunoreactivity was detected in spermatogonia (Figure 1B, Supplementary Figure 4). A very faint labeling was observed in primary spermatocytes, appearing as few puncta in the nucleus (Figure 1B, Supplementary Figure 5). In round spermatids, hCRISP2 immunoreactivity in the nucleus was more intense and homogeneous than in primary spermatocytes (Figure 1B, Supplementary Figures 6 and 7). In early elongated spermatids, some intense spots of hCRISP2 immunoreactivity were observed in the nucleus, accompanied by a labeling in the cytoplasm (Figure 1B, Supplementary Figure 8). Finally, in late elongated spermatids, hCRISP2 was observed within the equatorial segment of the acrosome (EqS), in the cytoplasm, and in the flagellum (Figure 1B, Figure 2, Supplementary Figure 9). Elongated spermatids displaying immunostained cytoplasm were found at the apical pole of the Sertoli cells. Additionally, small puncta of hCRISP2 immunoreactivity were observed in the nucleus and cytoplasm of Sertoli cells (Figure 1, Supplementary Figure 10). The control experiments, where the primary antibody was omitted, revealed no labeling on the testis sections (Supplementary Figure 11).

As the other two members of the human CRISP family, hCRISP1 and 3, are expressed and secreted by the epididymal epithelium (cf. Supplementary Figure 12A for hCRISP1), and considering hCRISP2 possesses a signal peptide, we investigated whether hCRISP2 is also expressed at epididymal level. Results showed that hCRISP2 immunostaining was restricted to the sperm present in the lumen of the epididymis, as an intense dense spot at the basal region of the head, and at the level of the flagellum, with no labeling observed in epithelial cells (Figure 3, Supplementary Figure 12B). The control experiments, where the primary antibody was omitted, revealed no labeling on the epididymis sections (Supplementary Figure 12C).

### Localization of hCRISP2 on ejaculated sperm before and after capacitation and acrosome reaction

We investigated hCRISP2 localization in mature ejaculated sperm before and after capacitation and AR using PSA-FITC labeling to assess acrosome integrity. For analysis of the AR, we compared the effects of induction with calcium ionophore (A23187) with those produced by a more physiological induction using progesterone. Independently of the tested condition, hCRISP2 was consistently detected as an intense spot in the basal region of the head in all sperm (Figure 4, Supplementary Figure 13). A labeling was also observed in the flagellum of almost all (>90%) sperm. In both non-capacitated and capacitated sperm, a weak signal was additionally detected in the apical region of the head and at the level of the EqS (Figure 4, Supplementary Figure 13). Based on PSA-FITC labeling, the calcium ionophore was more potent than the progesterone to induce AR. In acrosome-reacted sperm (i.e., no or EqS-restricted PSA-FITC labeling), different results were observed regarding hCRISP2 immunoreactivity in the apical region and EqS, depending on the sperm. While many still exhibited hCRISP2 immunoreactivity at the EqS, some showed no labeling in the apical region, while others retained it (Figure 4, Supplementary Figure 13). Notably, we tested two methods of epitope retrieval (ER) on sperm to improve accessibility of the antibodies to native hCRISP2: (1) HIER (heat-induced epitope retrieval), where sperm were incubated in citric acid, with or without EDTA, heated at 95°C, and (2) RTER (room temperature epitope retrieval), where sperm were incubated in 10% formic acid or 2 N HCl. However, these did not change the results (data not shown). In addition, we tried a method of signal amplification using biotinylated secondary antibodies and streptavidin–Texas red, but again with no change in the results obtained (data not shown).

### Identification of hCRISP2 isoform in sperm

In the public Ensembl database, three transcripts are listed for hCRISP2 (referred to as CRISP2-201, CRISP2-202, and CRISP2-203), encoding two potential protein isoforms that differ by only 35 amino acids encoded by exon 9. Transcripts CRISP2-201 and CRISP2-202 only differ in the 5′ untranslated region. CRISP2-201 encodes for a 243-amino-acid isoform with a calculated molecular weight of 27.3 kDa, designated in UniProt as P16562-1, while transcript CRISP2-203 encodes for a 278-amino-acid isoform with a calculated molecular weight of 31.6 kDa, designated in UniProt as P16562-2. To check if both isoforms are present in sperm, we searched for hCRISP2 peptides in a sperm proteome available in our laboratory, obtained as detailed in the Materials

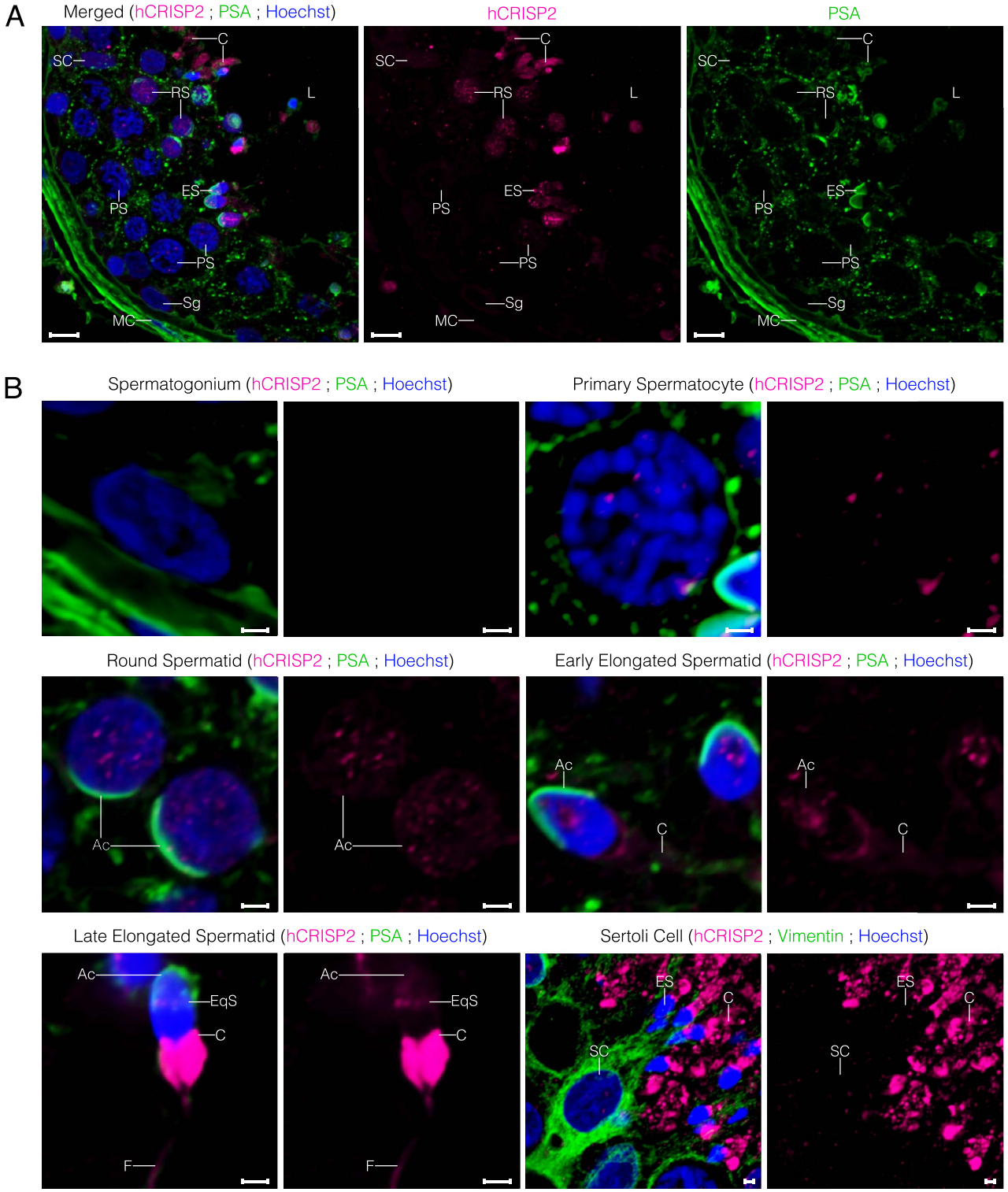


**Figure 1.** Localization of hCRISP2 on human testis sections. (A) Maximum-intensity projections (MaxIP) obtained from z-stack images using Nikon NIS Elements software. (B) Equatorial views of each cell type extracted from the z-stack images. Hoechst staining was used to label the nuclei, PSA-FITC staining was used to visualize sperm acrosomes, and vimentin immuno-labeling was used to highlight Sertoli cells. Scale bar: 10 $\mu$m in (A), 2 $\mu$m in (B). Ac, acrosome; C, cytoplasm; EqS, equatorial segment; ES, elongated spermatid; F, flagellum; L, lumen of the seminiferous tubule; MC, myoid cell; PS, primary spermatocyte; RS, round spermatid; SC, Sertoli cell; Sg, spermatogonium. Representative results from $N = 3$ replicates. Results from two other replicates and controls are available in Supplementary Figure 3 and Supplementary Figure 11, respectively.

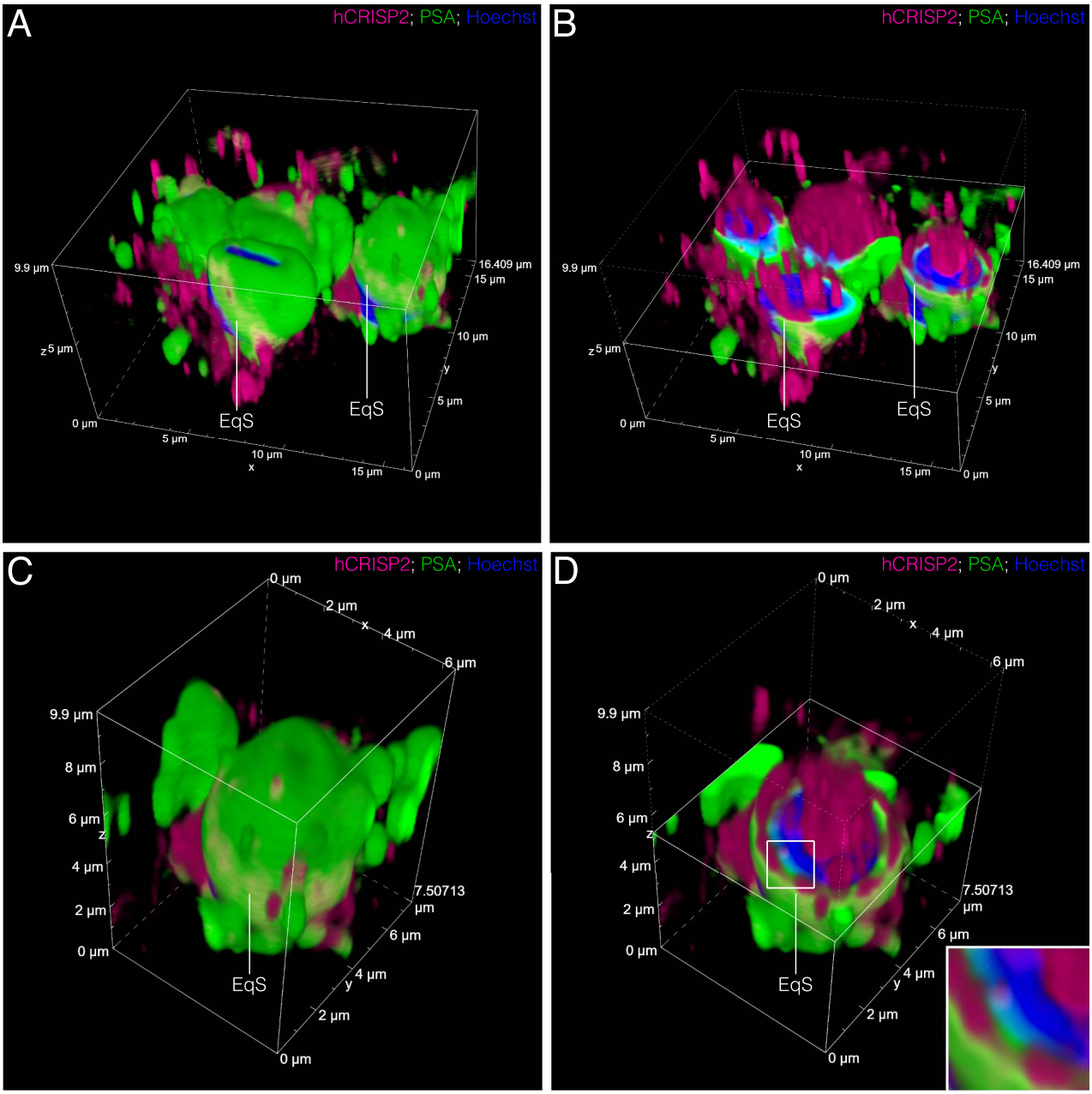


**Figure 2.** Three-dimensional (3D) reconstructions of elongated spermatids showing the intra-nuclear and intra-acrosomal (at the EqS) localization of hCRISP2. Three-dimensional rendered confocal z-stacks were obtained using Nikon NIS Elements software. Full renderings are shown in panels (A) and (C). For better clarity, partial renderings with orthogonal planar sectioning applied along the *z*-axis, leaving the hCRISP2 channel unaffected, are shown in panels (B) and (D). Panel (D) includes an inset that provides a detailed examination of the successive layers in the EqS region. Hoechst staining was used to label the nuclei and PSA-FITC staining was used to visualize sperm acrosomes. The scale is shown on the edge of the box enclosing the spermatid(s). EqS, equatorial segment.

and Methods section and in MS/MS results obtained from immunoprecipitated hCRISP2. A total of 18 distinct peptides were identified with >99% confidence, covering 54.05% and 46.69% of P16562-1 and P16562-2 isoforms, respectively (this calculation was performed excluding the signal peptide) (Figure 5). No peptide was identified within the protein region specific to isoform P16562-2 (i.e., encoded by exon 9), although identifiable tryptic peptides were predicted in this region. However, a peptide overlapping with the protein sequences encoded by exons 8 and 10 and, thus, totally specific to isoform P16562-1, was detected (Figure 5, Supplementary Figure 14).

## Extractability of hCRISP2 from sperm

Western blot analysis of sperm extracts obtained in denaturing conditions (i.e., in the presence of 2% SDS and 100 mM DTT) revealed the presence of hCRISP2 as a unique band of ~25 kDa (Supplementary Figure 2A). To analyze hCRISP2 extractability from sperm, frozen–thawed purified (considered as "non-capacitated") and capacitated sperm were sequentially extracted in PBS, PBS supplemented with 1% Triton X-100 (PBS-T), PBS-T supplemented with 0.5% sodium deoxycholate (PBS-T-D), and, finally, with Laemmli SDS sample buffer (SB). SDS-PAGE and WB analysis of the extracts revealed that, by considering the cumulated intensity

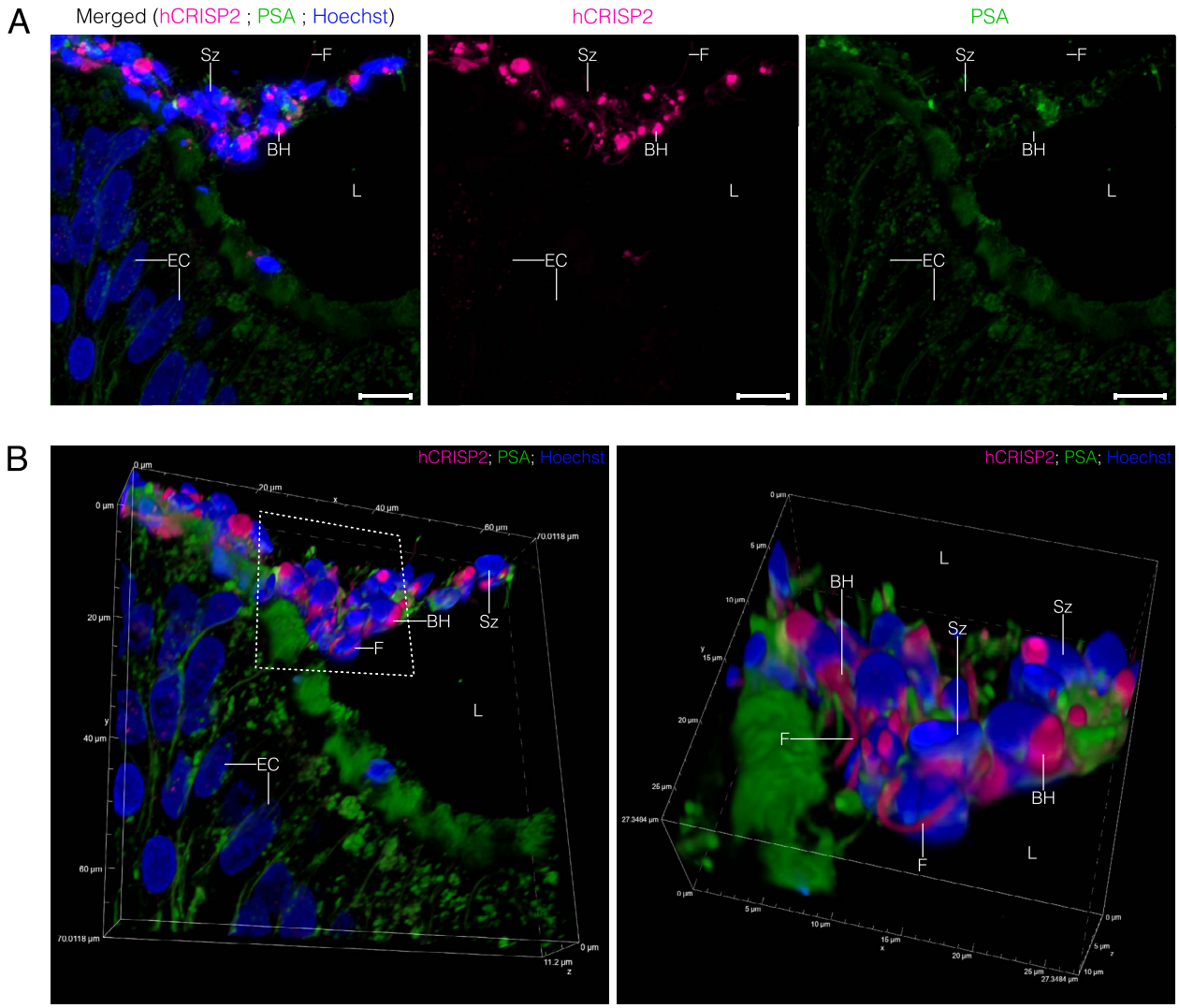


**Figure 3.** Localization of hCRISP2 on human epididymis sections. (A) Maximum-intensity projections (MaxIP) obtained from z-stack images using Nikon NIS Elements software. Scale bar: 10 $\mu$m. (B) Three-dimensional (3D) rendered confocal z-stacks, general view on the left and detailed view on the right. The scale is shown on the edge of the box enclosing the 3D rendering. Hoechst staining was used to label the nuclei and PSA-FITC staining was used to visualize sperm acrosomes. Scale bar: 10 $\mu$m. BH, basal region of the head; EC, epithelial cell; F, flagellum; L, lumen of the epididymis; Sz, sperm. Representative results from $N = 2$ replicates. Results from another replicate, corresponding general views, and controls are available in Supplementary Figure 12.

of hCRISP2 immunostaining in the different conditions as 100%, ~65% and 91% of hCRISP2 were extracted using PBS from the purified or capacitated sperm, respectively (Figure 6). For purified, non-capacitated sperm, subsequent incubation with PBS-T was necessary to extract an additional fraction (34%) of hCRISP2 (Figure 6).

## Analysis of hCRISP2 quaternary organization

Native-PAGE and WB analysis of sperm extracts obtained in PBS from purified (considered as "non-capacitated") and capacitated sperm detected hCRISP2 as three high molecular weight bands (Figure 7). This electrophoretic pattern was also observed after immunoprecipitation (IP) of hCRISP2 from both non-capacitated and capacitated sperm (Figure 7), and irrespective of the extraction method used. Specifically, similar patterns were observed when sperm were fresh or frozen–thawed, lysed using PBS associated or not to sonication or Triton X-100, and in the presence or absence of DTT (Supplementary Figure 15). However, the bands obtained were of very low intensity when fresh samples were extracted with PBS only (Supplementary Figure 15). Interestingly, the high molecular weight hCRISP2 complexes were not disrupted at high concentrations of NaCl, DTT, EDTA, Triton X-100, or urea (Supplementary Figure 16).

To investigate the composition of the complexes formed by hCRISP2, the eluate obtained after hCRISP2 immunoprecipitation was analyzed by mass spectrometry. The experiment was performed with three independent samples (three replicates), and the results were compared to three control conditions (Dynabeads without any antibody, or coupled to rabbit IgG isotype or to a different rabbit polyclonal antibody, in this case directed against HSP70). Excepted for contaminant proteins (i.e., either proteins non-specifically linked to the resin and common with the control conditions, or keratin and antibody fragments), the eluate obtained after hCRISP2 immunoprecipitation was only made up of hCRISP2 in two out of the three replicates. In the third replicate, beta-microseminoprotein co-eluted with hCRISP2.

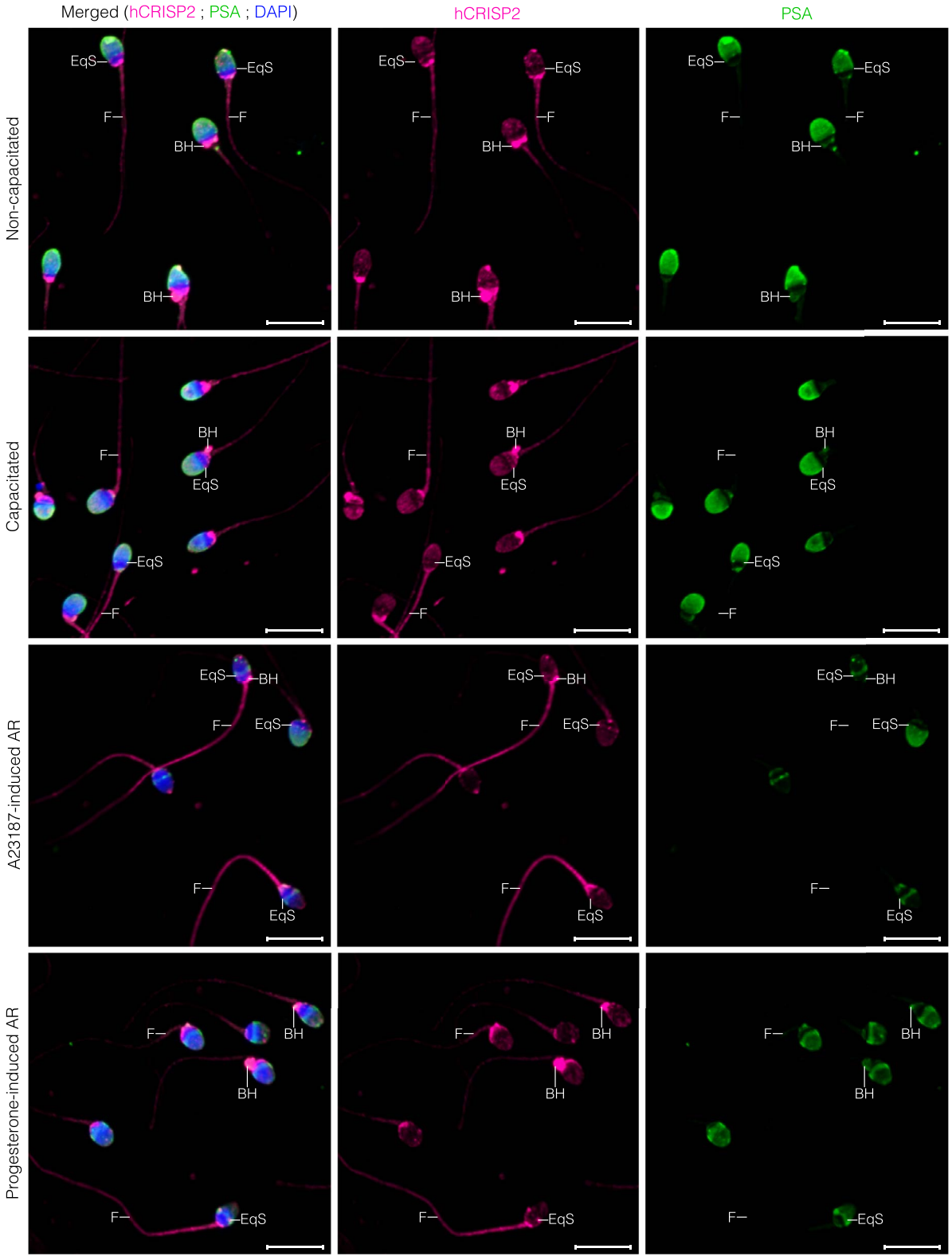


**Figure 4.** Localization of hCRISP2 within human sperm, before and after capacitation as well as after acrosomal reaction (AR) induced either by calcium ionophore (A23187) or progesterone. Images are maximum-intensity projections (MaxIP) obtained from z-stack images using Nikon NIS Elements software. DAPI staining was used to label the nuclei and PSA-FITC staining was used to label the acrosomes. Scale bar: 10 $\mu$m. BH, basal region of the head; EqS, equatorial segment; F, flagellum. General views and control are available in Supplementary Figure 13. Representative results from $N = 3$ replicates.


**Figure 5.** Identification of hCRISP2 isoform in human sperm. Peptides identified by mass spectrometry from hCRISP2 immunoprecipitated from ejaculated sperm are aligned on the two hCRISP2 isoforms listed in UniProt (P16562-1 and P16562-2). Translation of the longest mRNA coding for hCRISP2 from Ensembl database (CRISP2-203) is shown to highlight coding exons. The alignment was performed using Geneious software. Exon-encoded regions, the protein sequence encoded by hCRISP2 ORF, hCRISP2 peptide signal, and peptides identified in mass spectrometry are shown. The peptide overlapping the protein sequences encoded by exons 8 and 10 and specific to isoform P16562-1 (fragmentation spectrum and fragment ions table are available in Supplementary Figure 14) is indicated by a triangle.

This protein was not detected in any of the control eluates (Supplementary Table 2).

## Analysis of hCRISP2 post-translational modifications

The presence of post-translational modifications (PTMs) on hCRISP2 was investigated using lectin blot and WB to detect glycosylation and tyrosine phosphorylation, respectively. These experiments were performed on capacitated sperm as this process is known to involve protein PTMs [57]. In addition to immunoprecipitated hCRISP2, crude extracts obtained in Laemmli SDS sample buffer were analyzed to confirm the ability of the lectins and antibody to detect the corresponding PTMs. The presence of hCRISP2 was confirmed in both crude and immunoprecipitated extracts. In addition, a signal was detected using the lectins and the anti-phosphotyrosine antibody in the crude extracts, demonstrating the method's efficiency in detecting the corresponding PTMs in sperm.

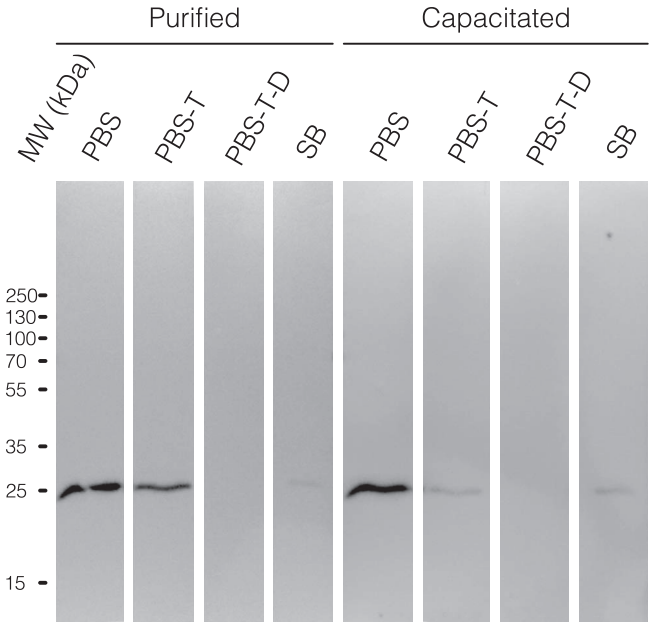


**Figure 6.** Detection of hCRISP2 in sperm extracts. Frozen–thawed purified and capacitated sperm were successively extracted with PBS, PBS supplemented with 1% Triton X-100 (PBS-T), PBS-T supplemented with 0.5% sodium deoxycholate (PBS-T-D), and Laemmli SDS sample buffer (SB), all containing protease and phosphatase inhibitors. Proteins from the supernatants of the different extracts were resolved by SDS-PAGE on a single gel (12% acrylamide) and analyzed by western blot using monoclonal anti-hCRISP2. Notably, a loading control is not included in these experiments, as variability in the intensity of the control protein is expected due to the different extraction buffers used sequentially.

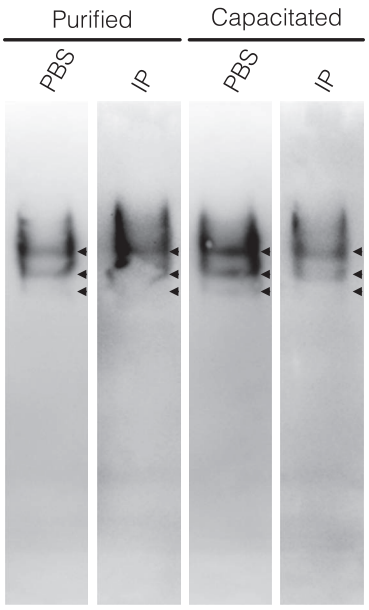


**Figure 7.** Electrophoretic mobility of hCRISP2. Proteins were extracted from purified or capacitated sperm under native condition (PBS) and a fraction of the lysate was used to immunoprecipitate hCRISP2 (IP). Both PBS and IP fractions were resolved by Native-PAGE (10% acrylamide) followed by western blot analysis using polyclonal anti-hCRISP2. Arrowheads indicate the three immunoreactive bands. Representative results from $N = 3$ replicates.

However, no signal was observed in the immunoprecipitated fractions, indicating the absence of detectable glycosylation and tyrosine phosphorylation on hCRISP2 (Figure 8).

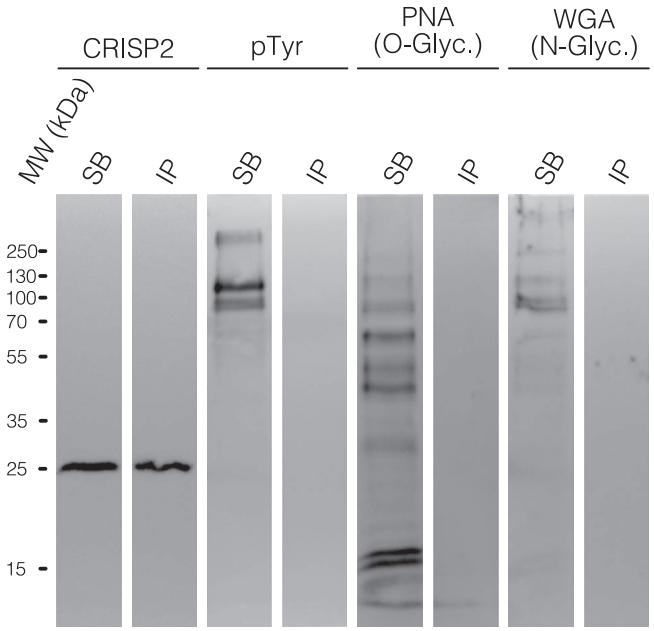


**Figure 8.** Analysis of hCRISP2 post-translational modifications. Crude extracts from capacitated sperm were obtained in Laemmli SDS sample buffer (SB) and hCRISP2 was immunoprecipitated in native conditions from capacitated sperm extracted with PBS (IP). The crude SB extract and IP eluate were separated by SDS-PAGE (12% acrylamide) and analyzed in western blot using anti-hCRISP2 to confirm the presence of hCRISP2 in the extracts, anti-phosphotyrosine (pTyr) antibodies to detect tyrosine phosphorylation, the lectin peanut agglutinin (PNA) to detect O-glycosylation, and the lectin wheat germ agglutinin (WGA) to detect N-glycosylation. The SB crude extract was analyzed to confirm the ability of the antibodies and lectins to detect the corresponding modifications. Representative results from $N = 4$ replicates.

## Discussion

Of the four CRISPs identified in mammals, CRISP2 stands out as the sole intracellular member, expressed specifically in the testis during spermatogenesis. It has gained attention because of its multiple roles in male fertility, including interaction with Sertoli cells during spermatogenesis [7, 27], sperm motility [9, 32, 33], and interaction with the oocyte [34, 35]. For these reasons, and given its expression exclusively limited to the testes, CRISP2 appears as a key protein in reproduction. However, although CRISP2 has been extensively studied in rodents and boars, data on human CRISP2 (hCRISP2) remains limited. Therefore, we aimed to deepen our understanding of hCRISP2 and its roles in human reproduction by analyzing its localization throughout spermatogenesis and epididymal maturation, as well as by exploring several of its molecular features.

### 1. *Human CRISP2 localization throughout spermatogenesis, epididymal maturation and in ejaculated sperm*

As highlighted in Supplementary Table 1, many studies investigated CRISP2 localization in the male reproductive system, but with results varying depending on the species, and even depending on the study within the same species (Supplementary Table 1). One of the reasons for this disparity could be experimental due to the use of different antibodies, tissue fixation, or treatment applied to testicular sections. Here, we made sure that the anti-CRISP2 we used could specifically target hCRISP2: (1) it labeled HeLa

cells expressing hCRISP2 but not hCRISP1, (2) its use in immunoprecipitation allowed the recovery of hCRISP2 only (Supplementary Table 2), and (3) Zhang [44] used the same antibody to study CRISP2 localization in boar sperm and showed no labeling when the antibody was pre-incubated with a blocking peptide. We used this same antibody to investigate the localization of hCRISP2 on testis sections, epididymis sections, and ejaculated sperm to enable a comparison of the results. In testes, hCRISP2 immunoreactivity was observed within the germ cell lineage, as already documented in rats [27, 28], humans [29, 30], and boars [31]. We observed a gradient of increasing signal intensity from primary spermatocytes to elongated spermatids. These results, which suggest hCRISP2 translation from the primary spermatocyte stage, are in line with accumulated data on CRISP2 mRNA expression in mice, rats, and humans, evaluated using in situ hybridization and single-cell RNA-seq, which indicate the appearance of CRISP2 mRNA transcripts in pachytene spermatocytes with levels increasing progressively through subsequent stages [1, 27, 30, 58–60].

Human CRISP2 initially appears in the nucleus of primary spermatocytes and round spermatids. It is still observed in the nucleus of early elongated spermatids but becomes undetectable in the nucleus of late elongated spermatids. This absence of nuclear labeling in late elongated spermatids may result from high chromatin condensation at this stage, likely restricting antibody access to hCRISP2. To the best of our knowledge, the presence of hCRISP2 in the nucleus of primary spermatocytes and spermatids is reported for the first time. This immunostaining is most likely specific as no labeling was observed in the nucleus of other cell types (i.e., myoids and spermatogonia), excepted for Sertoli cells, in which a faint labeling was observed. The presence of hCRISP2 inside the nucleus appears atypical, as no nuclear localization signal (NLS) has been identified or predicted in hCRISP2. However, the absence of an NLS does not preclude nuclear entry of proteins. For example, proteins smaller than ~40–60 kDa can passively diffuse through the nuclear pore complex, and some proteins may also enter by binding to other proteins that have an NLS [61]. To accurately determine hCRISP2 localization within the nucleus, higher-resolution techniques, such as immuno-TEM, should be employed. Currently, it is challenging to propose a specific role for hCRISP2 within the nucleus of spermatocytes and spermatids. It is known that the nucleus plays a role in the quality control of cytoplasmic proteins [62]. Therefore, it is possible that some misfolded hCRISP2 are targeted to the nucleus for degradation or sequestration. Further studies are necessary to investigate this possibility and clarify the role of hCRISP2 in the nucleus. Interestingly, the proteome of the human sperm nucleus includes many proteins traditionally considered non-nuclear, such as CRISP1 [63]. In mice, one such protein, ACTL7A, a protein from the perinuclear theca (PT), displays a localization pattern during spermatogenesis similar to that of hCRISP2. It is predominantly nuclear in spermatocytes and round spermatids but shifts to a cytoplasmic localization in elongated spermatids [64]. Small puncta of hCRISP2 immunoreactivity were also detected in the nucleus of Sertoli cells. Since Sertoli cells absorb the residual cytoplasm expelled by maturing spermatids, a plausible explanation for this nuclear labeling is that some hCRISP2 mRNA may be translated within these cells, with hCRISP2 subsequently localizing in their nucleus, similar to its behavior in spermatocytes and spermatids. In addition to the nucleus, hCRISP2 was observed in the cytoplasm of early elongated spermatids and was subsequently observed within the EqS and in the flagellum of late elongated spermatids. Some aggregated material with hCRISP2 immunoreactivity was also observed in apical extensions of Sertoli cells. This material likely corresponds to apoptotic spermatogenic cells or residual bodies, cytoplasmic remnants of the spermatids which are phagocytized by Sertoli cells during spermiogenesis and spermiation [65–67]. Similar results were described in rats regarding the presence of rCRISP2 in the cytoplasm of elongating spermatids and its incorporation in the flagellum [28]. Interactions of CRISP2 with proteins like mitogen-activated protein kinase kinase kinase 11 (MAP3K11) [36], gametogenetin 1 (GGN1) [37], and sperm head and tail associated protein (SHTAP) [38] suggest its involvement in the formation of essential sperm structures such as the acrosome or the flagellum during spermatogenesis. Once these structures are formed, this subpopulation of CRISP2 may no longer be necessary and thus eliminated. In rats, rCRISP2 immunoreactivity is detectable in the acrosome starting at the round spermatid stage [28]. In contrast, we did not observe hCRISP2 in the forming acrosome. However, the presence of hCRISP2 within the EqS suggests that it may be present in small quantities during acrosome formation, making it difficult to detect in our analyses. Human CRISP2 localization in the acrosome was expected, given the presence of a signal peptide at its N terminus, which typically directs it into the secretory network. However, its presence in cytoplasmic compartments is more surprising and difficult to explain. Noteworthy, phenomena of retro-translocation have been described in the literature for proteins with improper folding [68]. In such cases, misfolded proteins in the ER are transported to the cytosol for degradation by the proteasome [68]. Therefore, it is possible that some misfolded hCRISP2 undergoes such translocation to the cytoplasm, where the proteasome is localized.

Given that all other CRISPs are secreted by the epididymal epithelium and the presence of a signal peptide in CRISP2, we investigated hCRISP2 expression in human epididymal sections. The absence of labeling in epididymal cells confirmed the testis specificity of hCRISP2 expression [2]. Sperm within the epididymal lumen presented an intense labeling at the basal region of the head and along the flagellum. However, contrary to late elongated spermatids, the last germ cell stage observed in the testis sections, these sperm did not present any hCRISP2 immunoreactivity at the EqS. Noteworthy, PSA-FITC labeling of the acrosomes was also absent on epididymis sections, indicating a potential bias during the experimentation.

Finally, we investigated hCRISP2 localization in mature ejaculated sperm before and after capacitation, and after AR. Human CRISP2 was consistently detected as an intense spot at the basal region of the head, which likely corresponds to the cytoplasmic droplet, a tiny portion of cytoplasm retained after spermiogenesis and spermiation [69, 70]. In this cytoplasm compartment is localized the redundant nuclear envelope (RNE) that serves as a calcium reservoir essential for sperm motility [71–73]. Studies have shown CRISP2 interaction with ryanodine channel receptors [9], which regulate calcium flux and are also located at the base of the head [74, 75]. Human CRISP2 was also present within the flagellum of ejaculated sperm, which is coherent with studies showing its ability to interact with CatSper [33] and its localization in the outer dense fibers and longitudinal columns of the fibrous sheets of

the flagellum in other species [28, 44, 58]. In addition, a signal was observed in the apical region of the head and at the level of the EqS region in both non-capacitated and capacitated sperm. Since labeling of the apical region was not observed in elongated spermatids in testis sections, it could be non-specific, possibly due to antibody adsorption in this region. The apical membrane of ejaculated sperm undergoes modifications compared to spermatids [76], which may account for this. As for the signal at the EqS region, it is likely that it is present within the acrosome, as observed in elongated spermatid. Our results, therefore, do not seem to show the presence of hCRISP2 in the PT, as observed in boars [44, 45, 48]. However, as sperm spread on slides are relatively flat, we were not able to obtain correct 3D reconstructions with confocal imaging. Higher-resolution techniques, such as immuno-TEM, should be used to confirm our hypothesis. Although our results are consistent with the observations made by Anklesaria [43] and Du [29] in humans, they diverge from studies by Busso [34] and Nimlamool [42], where an intense hCRISP2 immunoreactivity was predominantly observed in the acrosome in non-capacitated and capacitated sperm. The use of different antibodies and/or protocols could explain these differences.

Following the AR, most sperm continued to display a labeling at the EqS, whereas immunostaining of the apical region of the head was variable, appearing in some sperm but absent in others. The presence of hCRISP2 at the EqS after AR is in line with previous studies on human sperm [34, 42]. However, in this study, we show that hCRISP2 is already present at the EqS before the AR, in contrast to other studies that reported hCRISP2 initially localized in the whole acrosome and relocated to the EqS [34, 42] after the AR. However, this location in the EqS (i.e., sandwiched between the remaining outer and inner acrosomal membranes) is not compatible with CRISP2's described role in fusion with the oocyte [32, 33, 35, 77], which implies its presence on the plasma membrane covering the EqS region. The presence of hCRISP2 at the surface of the EqS following AR could correspond to a fraction of acrosomal hCRISP2 reassociating to this location, as proposed by Busso [30] and Nimlamool [36]. Alternatively, hCRISP2 could be associated to the acrosome membranes of the EqS through binding to a membrane protein and relocate at the surface of the EqS region during AR, as proposed in the so-called lateral diffusion model for equatorin [78].

### 2. *Molecular characterization of hCRISP2*

Although two hCRISP2 isoforms are identified in databases (P16562-1 and -2 in UniProt), it is usually assumed that the shorter one, P16562-1, is the one expressed in sperm. However, to the best of our knowledge, no studies attempted to prove it experimentally. These two isoforms differ by the presence of 35 additional amino acids in P16562-2. Here, we analyzed sperm extracts by WB using two different anti-hCRISP2, one mouse monoclonal, and one rabbit polyclonal. Both antibodies revealed a band at ~25 kDa, corresponding to the shorter isoform of hCRISP2 without its signal peptide. We also searched for hCRISP2 peptides in a proteome of human sperm available in our laboratory and in MS/MS data obtained from immunoprecipitated hCRISP2. No peptide was detected in the 35-amino-acid region specific to P16562-2 isoform, although identifiable tryptic peptides were predicted in this region. In contrast, a peptide overlapping the sequences framing this region, and specific to P16562-1 isoform, was identified. These results strongly suggest that the shorter isoform of hCRISP2 predominates in sperm. However, the potential presence of the longer isoform cannot be entirely ruled out, as it may exist in a very small proportion, making it difficult to detect. Interestingly, no peptide corresponding to the signal peptide of hCRISP2 was detected, suggesting that it is co-translationally cleaved.

Using sequential extraction in different buffers, we showed that most of hCRISP2 could be extracted from freeze–thawed sperm using PBS, or from fresh sperm using PBS supplemented with Triton-X-100, without the need for the addition of denaturing agents or detergents. We also noticed that hCRISP2 was more easily extracted from capacitated sperm than from non-capacitated sperm. Indeed, all three processes (freezing, capacitation, and Triton X-100) are known to alter sperm membrane integrity [79–82]. These results indicate that hCRISP2 is present in easily accessible compartments after membrane breaking within sperm, such as the acrosome or the cytoplasmic droplet, as observed in IF in the present study. This is contrasting to results obtained in boar sperm, in which CRISP2 was found in the detergent-resistant PT and flagellum [44]. However, some additional hCRISP2 could be extracted after subsequent incubation in Laemmli SDS sample buffer, which could correspond to more stabilized proteins, such as those present in the flagellum or RNE.

After extraction in PBS and Native-PAGE analysis, hCRISP2 migrated as three high molecular weight bands. Concerned about potential aggregate formation induced by sonication [83] and freezing [84], we omitted these steps in sample preparation, but observed no impact. The presence of CRISP2 complexes was also observed in boar sperm head and flagellum extracts [44]. However, in this species, these flagellar complexes were maintained in denaturing conditions (SDS-PAGE), which was not the case in the present study. To identify the type of interactions stabilizing these aggregates, we incubated sperm PBS extracts with high concentrations of various agents targeting specific interactions (urea, DTT, NaCl, EDTA, or Triton X-100). However, none of these conditions resulted in the dissociation of the aggregates. These results show that hCRISP2 forms highly stabilized complexes in sperm. However, we cannot rule out the fact that the agents may have been washed away during electrophoresis, preventing their dissociative effect. Analysis of these complexes in mass spectrometry after IP revealed that they were only made up of hCRISP2 in two out of the three investigated replicates. In the third replicate, however, beta-microseminoprotein co-eluted with hCRISP2 and was not detected in any of the controls. This protein is secreted by the epithelial cells of the prostate and could potentially correspond to a contaminant during the IP procedure, given it was detected only in one of the three replicates. Our results contrast to findings in boars, where CRISP2 appears to interact with acrosin (ACR) and acrosin binding protein (ACRBP) [85]. In their study, Zhang et al. [85] identified 272 proteins in the eluate after CRISP2 IP while we identified only 8–12 proteins, according to the replicate. These differences could be attributed to the fact that we performed the IP using a lower amount of starting protein extract, a slightly lower-resolution mass spectrometer, and a gentler protein extraction protocol. Nonetheless, we identified hCRISP2 with up to 21 peptides, compared to the 17 peptides identified for boar CRISP2, indicating that our IP procedure is highly efficient despite the reduced starting material. In addition,

in the three negative control IPs omitting anti-hCRISP2, ACR and ACRBP were identified in the eluates, indicating that these proteins are non-specific contaminants in the IP process. Taken together, these findings suggest that the highly stabilized complexes formed by hCRISP2 are most likely composed solely of hCRISP2. These results are in line with observations that members of the CRISP family tend to form amyloid fibers [86, 87], which are fibrillar structures composed of identical proteins stacked on top of each other [88, 89]. These structures are thermodynamically stable and require harsh conditions for complete dissociation [90, 91]. While these amyloids are implicated in various pathologies [92, 93], they are not always harmful; in some cases, they play essential roles in processes like reproduction, gamete biology, and gamete interaction [94]. Nevertheless, it is not excluded that hCRISP2 could interact with other proteins (such as MAP3K11 or CatSper, cited previously) in the sperm. Indeed, our extraction method, compatible with immunoprecipitation and mass spectrometry, does not enable the extraction of all sperm proteins. The absence of detergent, for example, limits the extraction of membrane proteins. Post-translational modifications are important modulator of protein function in reproduction [95]. While CRISP1, 3, and 4 exhibit glycosylations [11, 22, 50–52], CRISP2 has always been described as lacking such PTMs. However, to the best of our knowledge, this assumption is based on a single study, conducted in guinea pigs [41]. Moreover, the presence of other PTMs on CRISP2 has never been considered. Here, using WB and lectin blot, we were not able to detect the presence of tyrosine phosphorylation and glycosylation on hCRISP2 immunoprecipitated from capacitated sperm. However, the possibility of potential PTMs cannot be entirely dismissed, as they might only impact a small fraction of the hCRISP2 pool, rendering them challenging to detect with the method used in the present study. Moreover, these modifications could be transient, further complicating their visualization. Noteworthy, during the last 20 years, PTM-specific proteomic studies allowed the identification of post-translationally modified proteins in sperm. A search of these proteomes supports the idea that CRISP2 does not exhibit glycosylations, while a few peptides exhibiting phosphoserine (a PTM not targeted in the present study) have been identified (Supplementary Table 3). The fact that hCRISP2 exhibits only minimal PTMs indicates that it does not primarily rely on these modifications to interact with other proteins during spermatogenesis or to fulfill its various functions. Notably, these minimal PTMs support the use of prokaryotic hosts for the recombinant production of hCRISP2 in further characterization studies.

Considering several reports showing significantly reduced levels of CRISP2 in infertile asthenozoospermic men [96–99], we believe that our observations on hCRISP2 expression, localization, and biochemical behavior provide important information for a better understanding of human infertility, as well as for future male contraceptive development.

## Acknowledgments

We thank P. Quenon from the Laboratory of Cell Biology in UMONS for technical assistance and all the technicians of the fertility clinic of the HELORA Hospital for their help in the recruitment of patients and voluntary donors.

## Supplementary material

Supplementary material is available at *BIOLRE* online.

**Conflict of interest:** The authors have declared that no conflict of interest exists.

## Data availability

The data underlying this article are available in the article and in its online supplementary material.

## Author contributions

EH, TM, PC, and PL conceptualized the research; EH acquired funding for the research; TM, AD, and MD performed the experiments and acquired data for the research; TM, BL, and EH developed the methodology of the research; EH was in charge of the research administration; DN, AF, JFS, VA, RW, and BL provided resources (materials, reagent, patient sample, instrumentation, and analysis tools) for the research; EH supervised the research; TM prepared the data for visualization; TM and EH wrote the original draft. All authors read, reviewed, and approved the final version of the manuscript.

## References

1. Mizuki N, Sarapata DE, Garcia-Sanz JA, Kasahara M. The mouse male germ cell-specific gene Tpx-1: molecular structure, mode of expression in spermatogenesis, and sequence similarity to two non-mammalian genes. *Mamm Genome* 1992; **3**:274–280.
2. Kratzschmar J, Haendler B, Eberspaecher U, Roosterman D, Donner P, Schleuning WD. The human cysteine-rich secretory protein (CRISP) family. Primary structure and tissue distribution of CRISP-1, CRISP-2 and CRISP-3. *Eur J Biochem* 1996; **236**:827–836.
3. Gibbs GM, Roelants K, O'bryan MK. The CAP superfamily: cysteine-rich secretory proteins, antigen 5, and pathogenesis-related 1 proteins—roles in reproduction, cancer, and immune defense. *Endocr Rev* 2008; **29**:865–897.
4. Gonzalez SN, Sulzyk V, Weigel Munoz M, Cuasnicu PS. Cysteine-rich secretory proteins (CRISP) are key players in mammalian fertilization and fertility. *Front Cell Dev Biol* 2021; **9**:800351.
5. Eberspaecher U, Roosterman D, Kratzschmar J, Haendler B, Habenicht UF, Becker A, Quensel C, Petri T, Schleuning WD, Donner P. Mouse androgen-dependent epididymal glycoprotein CRISP-1 (DE/AEG): isolation, biochemical characterization, and expression in recombinant form. *Mol Reprod Dev* 1995; **42**: 157–172.
6. Guo M, Teng M, Niu L, Liu Q, Huang Q, Hao Q. Crystal structure of the cysteine-rich secretory protein stecrisp reveals that the cysteine-rich domain has a K+ channel inhibitor-like fold. *J Biol Chem* 2005; **280**:12405–12412.
7. Maeda T, Sakashita M, Ohba Y, Nakanishi Y. Molecular cloning of the rat Tpx-1 responsible for the interaction between spermatogenic and Sertoli cells. *Biochem Biophys Res Commun* 1998; **248**: 140–146.
8. Ellerman DA, Cohen DJ, Da Ros VG, Morgenfeld MM, Busso D, Cuasnicu PS. Sperm protein "DE" mediates gamete fusion through an evolutionarily conserved site of the CRISP family. *Dev Biol* 2006; **297**:228–237.
9. Gibbs GM, Scanlon MJ, Swarbrick J, Curtis S, Gallant E, Dulhunty AF, O'bryan MK. The cysteine-rich secretory protein domain of Tpx-1 is related to ion channel toxins and regulates ryanodine receptor Ca2+ signaling. *J Biol Chem* 2006; **281**:4156–4163.
10. Koppers AJ, Reddy T, O'bryan MK. The role of cysteine-rich secretory proteins in male fertility. *Asian J Androl* 2011; **13**: 111–117.
11. Jalkanen J, Huhtaniemi I, Poutanen M. Mouse cysteine-rich secretory protein 4 (CRISP4): a member of the CRISP family exclusively

expressed in the epididymis in an androgen-dependent manner. *Biol Reprod* 2005; **72**:1268–1274.
12. Nolan MA, Wu L, Bang HJ, Jelinsky SA, Roberts KP, Turner TT, Kopf GS, Johnston DS. Identification of rat cysteine-rich secretory protein 4 (Crisp4) as the ortholog to human CRISP1 and mouse Crisp4. *Biol Reprod* 2006; **74**:984–991.
13. Turunen HT, Sipila P, Krutskikh A, Toivanen J, Mankonen H, Hamalainen V, Bjorkgren I, Huhtaniemi I, Poutanen M. Loss of cysteine-rich secretory protein 4 (Crisp4) leads to deficiency in sperm-zona pellucida interaction in mice. *Biol Reprod* 2012; **86**: 1–8.
14. Haendler B, Kratzschmar J, Theuring F, Schleuning WD. Transcripts for cysteine-rich secretory protein-1 (CRISP-1; DE/AEG) and the novel related CRISP-3 are expressed under androgen control in the mouse salivary gland. *Endocrinology* 1993; **133**: 192–198.
15. Pathak BR, Breed AA, Deshmukh P, Mahale SD. Androgen receptor mediated epigenetic regulation of CRISP3 promoter in prostate cancer cells. *J Steroid Biochem Mol Biol* 2018; **181**:20–27.
16. Kohane AC, Pineiro L, Blaquier JA. Androgen-controlled synthesis of specific proteins in the rat epididymis. *Endocrinology* 1983; **112**: 1590–1596.
17. Charest NJ, Joseph DR, Wilson EM, French FS. Molecular cloning of complementary deoxyribonucleic acid for an androgen-regulated epididymal protein: sequence homology with metalloproteins. *Mol Endocrinol* 1988; **2**:999–1004.
18. Laine M, Porola P, Udby L, Kjeldsen L, Cowland JB, Borregaard N, Hietanen J, Stahle M, Pihakari A, Konttinen YT. Low salivary dehydroepiandrosterone and androgen-regulated cysteine-rich secretory protein 3 levels in Sjogren's syndrome. *Arthritis Rheum* 2007; **56**:2575–2584.
19. Bjartell A, Johansson R, Bjork T, Gadaleanu V, Lundwall A, Lilja H, Kjeldsen L, Udby L. Immunohistochemical detection of cysteine-rich secretory protein 3 in tissue and in serum from men with cancer or benign enlargement of the prostate gland. *Prostate* 2006; **66**:591–603.
20. Fedorka CE, Scoggin KE, Squires EL, Ball BA, Troedsson MHT. Expression and localization of cysteine-rich secretory protein-3 (CRISP-3) in the prepubertal and postpubertal male horse. *Theriogenology* 2017; **87**:187–192.
21. Thimon V, Frenette G, Saez F, Thabet M, Sullivan R. Protein composition of human epididymosomes collected during surgical vasectomy reversal: a proteomic and genomic approach. *Hum Reprod* 2008; **23**:1698–1707.
22. Udby L, Bjartell A, Malm J, Egesten A, Lundwall A, Cowland JB, Borregaard N, Kjeldsen L. Characterization and localization of cysteine-rich secretory protein 3 (CRISP-3) in the human male reproductive tract. *J Androl* 2005; **26**:333–342.
23. Cohen DJ, Ellerman DA, Busso D, Morgenfeld MM, Piazza AD, Hayashi M, Young ET, Kasahara M, Cuasnicu PS. Evidence that human epididymal protein ARP plays a role in gamete fusion through complementary sites on the surface of the human egg. *Biol Reprod* 2001; **65**:1000–1005.
24. Roberts KP, Ensrud-Bowlin KM, Piehl LB, Parent KR, Bernhardt ML, Hamilton DW. Association of the protein D and protein E forms of rat CRISP1 with epididymal sperm. *Biol Reprod* 2008; **79**:1046–1053.
25. Udby L, Cowland JB, Johnsen AH, Sørensen OE, Borregaard N, Kjeldsen L. An ELISA for SGP28/CRISP-3, a cysteine-rich secretory protein in human neutrophils, plasma, and exocrine secretions. *J Immunol Methods* 2002; **263**:43–55.
26. Schambony A, Gentzel M, Wolfes H, Raida M, Neumann U, Topfer-Petersen E. Equine CRISP-3: primary structure and expression in the male genital tract. *Biochim Biophys Acta* 1998; **1387**: 206–216.
27. Maeda T, Nishida J, Nakanishi Y. Expression pattern, subcellular localization and structure–function relationship of rat Tpx-1, a spermatogenic cell adhesion molecule responsible for association with Sertoli cells. *Dev Growth Differ* 1999; **41**:715–722.
28. O'bryan MK, Sebire K, Meinhardt A, Edgar K, Keah HH, Hearn MT, De Kretser DM. Tpx-1 is a component of the outer dense fibers and acrosome of rat spermatozoa. *Mol Reprod Dev* 2001; **58**:116–125.
29. Du Y, Huang X, Li J, Hu Y, Zhou Z, Sha J. Human testis specific protein 1 expression in human spermatogenesis and involvement in the pathogenesis of male infertility. *Fertil Steril* 2006; **85**: 1852–1854.
30. Jamsai D, Reilly A, Smith SJ, Gibbs GM, Baker HW, Mclachlan RI, De Kretser DM, O'bryan MK. Polymorphisms in the human cysteine-rich secretory protein 2 (CRISP2) gene in Australian men. *Hum Reprod* 2008; **23**:2151–2159.
31. Gao F, Wang P, Wang K, Fan Y, Chen Y, Chen Y, Ye C, Feng M, Li L, Zhang S, Wei H. Investigation into the relationship between sperm cysteine-rich secretory protein 2 (CRISP2) and sperm fertilizing ability and fertility of boars. *Front Vet Sci* 2021; **8**:653413.
32. Brukman NG, Miyata H, Torres P, Lombardo D, Caramelo JJ, Ikawa M, Da Ros VG, Cuasnicu PS. Fertilization defects in sperm from cysteine-rich secretory protein 2 (Crisp2) knockout mice: implications for fertility disorders. *Mol Hum Reprod* 2016; **22**: 240–251.
33. Lim S, Kierzek M, O'connor AE, Brenker C, Merriner DJ, Okuda H, Volpert M, Gaikwad A, Bianco D, Potter D, Prabhakar R, Strunker T, *et al.* CRISP2 is a regulator of multiple aspects of sperm function and male fertility. *Endocrinology* 2019; **160**:915–924.
34. Busso D, Cohen DJ, Hayashi M, Kasahara M, Cuasnicu PS. Human testicular protein TPX1/CRISP-2: localization in spermatozoa, fate after capacitation and relevance for gamete interaction. *Mol Hum Reprod* 2005; **11**:299–305.
35. Busso D, Goldweic NM, Hayashi M, Kasahara M, Cuasnicu PS. Evidence for the involvement of testicular protein CRISP2 in mouse sperm-egg fusion. *Biol Reprod* 2007; **76**:701–708.
36. Gibbs GM, Bianco DM, Jamsai D, Herlihy A, Ristevski S, Aitken RJ, Kretser DM. Cysteine-rich secretory protein 2 binds to mitogen-activated protein kinase kinase kinase 11 in mouse sperm. *Biol Reprod* 2007; **77**:108–114.
37. Jamsai D, Bianco DM, Smith SJ, Merriner DJ, Ly-Huynh JD, Herlihy A, Niranjan B, Gibbs GM, O'bryan MK. Characterization of gametogenetin 1 (GGN1) and its potential role in male fertility through the interaction with the ion channel regulator, cysteine-rich secretory protein 2 (CRISP2) in the sperm tail. *Reproduction* 2008; **135**:751–759.
38. Jamsai D, Rijal S, Bianco DM, O'connor AE, Merriner DJ, Smith SJ, Gibbs GM. A novel protein, sperm head and tail associated protein (SHTAP), interacts with cysteine-rich secretory protein 2 (CRISP2) during spermatogenesis in the mouse. *Biol Cell* 2009; **102**:93–106.
39. Munoz MW, Ernesto JI, Bluguermann C, Busso D, Battistone MA, Cohen DJ, Cuasnicu PS. Evaluation of testicular sperm CRISP2 as a potential target for contraception. *J Androl* 2012; **33**:1360–1370.
40. Kim KS, Foster JA, Gerton GL. Differential release of Guinea pig sperm acrosomal components during exocytosis. *Biol Reprod* 2001; **64**:148–156.
41. Hardy DM, Huang TT Jr, Driscoll WJ, Tung KK, Wild GC. Purification and characterization of the primary acrosomal autoantigen of Guinea pig epididymal spermatozoa. *Biol Reprod* 1988; **38**: 423–437.
42. Nimlamool W, Bean BS, Lowe-Krentz LJ. Human sperm CRISP2 is released from the acrosome during the acrosome reaction and re-associates at the equatorial segment. *Mol Reprod Dev* 2013; **80**: 488–502.
43. Anklesaria JH, Kulkarni BJ, Pathak BR, Mahale SD. Identification of CRISP2 from human sperm as PSP94-binding protein and generation of CRISP2-specific anti-peptide antibodies. *J Pept Sci* 2016; **22**:383–390.
44. Zhang M, Bromfield EG, Veenendaal T, Klumperman J, Helms JB, Gadella BM. Characterization of different oligomeric forms of CRISP2 in the perinuclear theca versus the fibrous tail structures of boar spermatozoa. *Biol Reprod* 2021; **105**:1160–1170.

45. Zhang M, Bromfield EG, Helms JB, Gadella BM. The fate of porcine sperm CRISP2 from the perinuclear theca before and after in vitro fertilization. *Biol Reprod* 2022; **107**:1242–1253.
46. Wittayarat M, Kiatsomboon S, Kupthammasan N, Tipkantha W, Yimprasert S, Thongphakdee A, Panyaboriban S. Detection of protein biomarkers relevant to sperm characteristics and fertility in semen in three wild Felidae: the flat-headed cat (Prionailurus planiceps), fishing cat (Prionailurus viverrinus), and Asiatic golden cat (Catopuma temminckii). *Animals (Basel)* 2024; **14**:1027. https://doi.org/10.3390/ani14071027.
47. Wittayarat M, Pukazhenthi BS, Tipkantha W, Techakumphu M, Srisuwatanasagul S, Panyaboriban S. CRISP protein expression in semen of the endangered Malayan tapir (Tapirus indicus). *Theriogenology* 2021; **172**:106–115.
48. Zhang M, Chiozzi RZ, Skerrett-Byrne DA, Veenendaal T, Klumperman J, Heck AJR, Nixon B, Helms JB, Gadella BM, Bromfield EG. High resolution proteomic analysis of subcellular fractionated boar spermatozoa provides comprehensive insights into perinuclear theca-residing proteins. *Front Cell Dev Biol* 2022; **10**:836208.
49. Keah HH, O'bryan MK, De Kretser DM, Hearn MT. Synthesis and application of peptide immunogens related to the sperm tail protein tpx-1, a member of the CRISP superfamily of proteins. *J Pept Res* 2001; **57**:1–10.
50. Lea OA, Petrusz P, French FS. Purification and localization of acidic epididymal glycoprotein (AEG): a sperm coating protein secreted by the rat epididymis. *Int J Androl* 1978; **1**:592–607.
51. Roberts KP, Johnston DS, Nolan MA, Wooters JL, Waxmonsky NC, Piehl LB, Ensrud-Bowlin KM, Hamilton DW. Structure and function of epididymal protein cysteine-rich secretory protein-1. *Asian J Androl* 2007; **9**:508–514.
52. Volpert M, Mangum JE, Jamsai D, D'sylva R, O'bryan MK, Mcintyre P. Eukaryotic expression, purification and structure/function analysis of native, recombinant CRISP3 from human and mouse. *Sci Rep* 2014; **4**:4217.
53. WHO. *WHO Laboratory Manual for the Examination and Processing of Human Semen*, 6th ed. Geneva: World Health Organization; 2021.
54. Nicholson CM, Abramsson L, Holm SE, Bjurulf E. Bacterial contamination and sperm recovery after semen preparation by density gradient centrifugation using silane-coated silica particles at different g forces. *Hum Reprod* 2000; **15**:662–666.
55. Martin FJ, Amode MR, Aneja A, Austine-Orimoloye O, Azov AG, Barnes I, Becker A, Bennett R, Berry A, Bhai J, Bhurji SK, Bignell A, *et al.* Ensembl 2023. *Nucleic Acids Res* 2023; **51**:D933–D941.
56. Bateman A, Martin M-J, Orchard S, Magrane M, Ahmad S, Alpi E, Bowler-Barnett EH, Britto R, Bye-a-Jee H, Cukura A, Denny P, Dogan T, *et al.* UniProt: the universal protein knowledgebase in 2023. *Nucleic Acids Res* 2023; **51**:D523–D531.
57. Martin-Hidalgo D, Serrano R, Zaragoza C, Garcia-Marin LJ, Bragado MJ. Human sperm phosphoproteome reveals differential phosphoprotein signatures that regulate human sperm motility. *J Proteomics* 2020; **215**:103654.
58. O'bryan MK, Loveland KL, Herszfeld D, Mcfarlane JR, Hearn MT, De Kretser DM. Identification of a rat testis–specific gene encoding a potential rat outer dense fibre protein. *Mol Reprod Dev* 1998; **50**:313–322.
59. Mahyari E, Vigh-Conrad KA, Daube C, Lima AC, Guo J, Carrell DT, Hotaling JM, Aston KI, Conrad DF. The human infertility single-cell testis atlas (HISTA): an interactive molecular scRNA-Seq reference of the human testis. *Andrology* 2024; 1–11. https://doi.org/10.1111/andr.13637.
60. Guo J, Nie X, Giebler M, Mlcochova H, Wang Y, Grow EJ, Donorconnect, Kim R, Tharmalingam M, Matilionyte G, Lindskog C, Carrell DT, *et al.* The dynamic transcriptional cell atlas of testis development during human puberty. *Cell Stem Cell* 2020; **26**:262–276.e4.
61. Cautain B, Hill R, De Pedro N, Link W. Components and regulation of nuclear transport processes. *FEBS J* 2015; **282**:445–462.
62. Borgert L, Mishra S, Den Brave F. Quality control of cytoplasmic proteins inside the nucleus. *Comput Struct Biotechnol J* 2022; **20**:4618–4625.
63. De Mateo S, Castillo J, Estanyol JM, Ballesca JL, Oliva R. Proteomic characterization of the human sperm nucleus. *Proteomics* 2011; **11**:2714–2726.
64. Ferrer P, Upadhyay S, Ikawa M, Clement TM. Testis-specific actin-like 7A (ACTL7A) is an indispensable protein for subacrosomal-associated F-actin formation, acrosomal anchoring, and male fertility. *Mol Hum Reprod* 2023; **29**:gaad005. https://doi.org/10.1093/molehr/gaad005.
65. Franca LR, Hess RA, Dufour JM, Hofmann MC, Griswold MD. The Sertoli cell: one hundred fifty years of beauty and plasticity. *Andrology* 2016; **4**:189–212.
66. Tung KSK, Harakal J, Qiao H, Rival C, Li JCH, Paul AGA, Wheeler K, Pramoonjago P, Grafer CM, Sun W, Sampson RD, Wong EWP, *et al.* Egress of sperm autoantigen from seminiferous tubules maintains systemic tolerance. *J Clin Invest* 2017; **127**:1046–1060.
67. Fei W, Daishu H. Sertoli cell phagocytosis: an essential event for spermatogenesis. In: Wei W, Francesco Z, Umberto M (eds.), *Male Reproductive Health*. IntechOpen: IntechOpen; 2019: Ch. 5.
68. Tsai B, Ye Y, Rapoport TA. Retro-translocation of proteins from the endoplasmic reticulum into the cytosol. *Nat Rev Mol Cell Biol* 2002; **3**:246–255.
69. Rengan AK, Agarwal A, Der Linde, Michelle, Plessis D, Stefan S. An investigation of excess residual cytoplasm in human spermatozoa and its distinction from the cytoplasmic droplet. *Reprod Biol Endocrinol* 2012; **10**:92.
70. Cooper TG, Yeung CH, Fetic S, Sobhani A, Nieschlag E. Cytoplasmic droplets are normal structures of human sperm but are not well preserved by routine procedures for assessing sperm morphology. *Hum Reprod* 2004; **19**:2283–2288.
71. Mata-Martinez E, Sanchez-Cardenas C, Chavez JC, Guerrero A, Trevino CL, Corkidi G, Montoya F, Hernandez-Herrera P, Buffone MG, Balestrini PA, Darszon A. Role of calcium oscillations in sperm physiology. *Biosystems* 2021; **209**:104524.
72. Ho HC, Suarez SS. Characterization of the intracellular calcium store at the base of the sperm flagellum that regulates hyperactivated motility. *Biol Reprod* 2003; **68**:1590–1596.
73. Finkelstein M, Etkovitz N, Breitbart H. Ca(2+) signaling in mammalian spermatozoa. *Mol Cell Endocrinol* 2020; **516**:110953.
74. Harper CV, Barratt CL, Publicover SJ. Stimulation of human spermatozoa with progesterone gradients to simulate approach to the oocyte. Induction of [Ca(2+)](i) oscillations and cyclical transitions in flagellar beating. *J Biol Chem* 2004; **279**:46315–46325.
75. Costello S, Michelangeli F, Nash K, Lefievre L, Morris J, Machado-Oliveira G, Barratt C, Kirkman-Brown J, Publicover S. Ca2+-stores in sperm: their identities and functions. *Reproduction* 2009; **138**:425–437.
76. Cornwall GA. New insights into epididymal biology and function. *Hum Reprod Update* 2009; **15**:213–227.
77. Curci L, Brukman NG, Weigel Munoz M, Rojo D, Carvajal G, Sulzyk V, Gonzalez SN, Rubinstein M, Da Ros VG, Cuasnicu PS. Functional redundancy and compensation: deletion of multiple murine Crisp genes reveals their essential role for male fertility. *FASEB J* 2020; **34**:15718–15733.
78. Yoshida K, Ito C, Yamatoya K, Maekawa M, Toyama Y, Suzuki-Toyota F, Toshimori K. A model of the acrosome reaction progression via the acrosomal membrane-anchored protein equatorin. *Reproduction* 2010; **139**:533–544.
79. Puga Molina LC, Luque GM, Balestrini PA, Marin-Briggiler CI, Romarowski A, Buffone MG. Molecular basis of human sperm capacitation. *Front Cell Dev Biol* 2018; **6**:72.
80. Cormier N, Bailey JL. A differential mechanism is involved during heparin- and cryopreservation-induced capacitation of bovine spermatozoa. *Biol Reprod* 2003; **69**:177–185.

81. Gautier C, Aurich C. "Fine feathers make fine birds" - the mammalian sperm plasma membrane lipid composition and effects on assisted reproduction. *Anim Reprod Sci* 2022; **246**:106884.
82. Mattei B, Lira RB, Perez KR, Riske KA. Membrane permeabilization induced by Triton X-100: the role of membrane phase state and edge tension. *Chem Phys Lipids* 2017; **202**:28–37.
83. Stathopulos PB, Scholz GA, Hwang YM, Rumfeldt JA, Lepock JR, Meiering EM. Sonication of proteins causes formation of aggregates that resemble amyloid. *Protein Sci* 2004; **13**: 3017–3027.
84. Wang W, Nema S, Teagarden D. Protein aggregation—pathways and influencing factors. *Int J Pharm* 2010; **390**:89–99.
85. Zhang M, Chiozzi RZ, Bromfield EG, Heck AJ, Helms JB, Gadella BM. Characterization of acrosin and acrosin binding protein as novel CRISP2 interacting proteins in boar spermatozoa. *Andrology* 2023; **11**:1460–1471.
86. Maldera JA, Vasen G, Ernesto JI, Weigel-Munoz M, Cohen DJ, Cuasnicu PS. Evidence for the involvement of zinc in the association of CRISP1 with rat sperm during epididymal maturation. *Biol Reprod* 2011; **85**:503–510.
87. Sheng J, Olrichs NK, Geerts WJ, Li X, Rehman AU, Gadella BM, Kaloyanova DV, Helms JB. Zinc binding regulates amyloid-like aggregation of GAPR-1. *Biosci Rep* 2019; **39**:BSR20182345. https://doi.org/10.1042/BSR20182345.
88. Willbold D, Strodel B, Schroder GF, Hoyer W, Heise H. Amyloid-type protein aggregation and prion-like properties of amyloids. *Chem Rev* 2021; **121**:8285–8307.
89. Chatani E, Yuzu K, Ohhashi Y, Goto Y. Current understanding of the structure, stability and dynamic properties of amyloid fibrils. *Int J Mol Sci* 2021; **22**:4349. https://doi.org/10.3390/ijms22094349.
90. Buell AK. Stability matters, too - the thermodynamics of amyloid fibril formation. *Chem Sci* 2022; **13**:10177–10192.
91. Sulatsky MI, Stepanenko OV, Stepanenko OV, Povarova OI, Kuznetsova IM, Turoverov KK, Sulatskaya AI. Broken but not beaten: challenge of reducing the amyloids pathogenicity by degradation. *J Adv Res* 2025; **70**:45–62. https://doi.org/10.1016/j.jare.2024.04.018.
92. Chiti F, Dobson CM. Protein misfolding, functional amyloid, and human disease. *Annu Rev Biochem* 2006; **75**:333–366.
93. Bashir S, Aiman A, Shahid M, Chaudhary AA, Sami N, Basir SF, Hassan I, Islam A. Amyloid-induced neurodegeneration: a comprehensive review through aggregomics perception of proteins in health and pathology. *Ageing Res Rev* 2024; **96**:102276.
94. Hewetson A, Do HQ, Myers C, Muthusubramanian A, Sutton RB, Wylie BJ, Cornwall GA. Functional amyloids in reproduction. *Biomolecules* 2017; **7**:3.
95. Samanta L, Swain N, Ayaz A, Venugopal V, Agarwal A. Post-translational modifications in sperm proteome: the chemistry of proteome diversifications in the pathophysiology of male factor infertility. *Biochim Biophys Acta* 2016; **1860**: 1450–1465.
96. Zhou JH, Zhou QZ, Yang JK, Lyu XM, Bian J, Guo WB, Chen ZJ, Xia M, Xia H, Qi T, Li X, Liu CD. MicroRNA-27a-mediated repression of cysteine-rich secretory protein 2 translation in asthenoteratozoospermic patients. *Asian J Androl* 2017; **19**: 591–595.
97. Manfrevola F, Ferraro B, Sellitto C, Rocco D, Fasano S, Pierantoni R, Chianese R. CRISP2, CATSPER1 and PATE1 expression in human asthenozoospermic semen. *Cells* 2021; **10**:1956, 1956. https://doi.org/10.3390/cells10081956.
98. Heidary Z, Zaki-Dizaji M, Saliminejad K, Khorramkhorshid HR. Expression analysis of the CRISP2, CATSPER1, PATE1 and SEMG1 in the sperm of men with idiopathic asthenozoospermia. *J Reprod Infertil* 2019; **20**:70–75.
99. Gholami D, Salman Yazdi R, Jami MS, Ghasemi S, Sadighi Gilani MA, Sadeghinia S, Teimori H. The expression of cysteine-rich secretory protein 2 (CRISP2) and miR-582-5p in seminal plasma fluid and spermatozoa of infertile men. *Gene* 2020; **730**: 144261.





*Biology of Reproduction*, 2025, 00, 1–18
https://doi.org/10.1093/biolre/ioaf051
Research Article

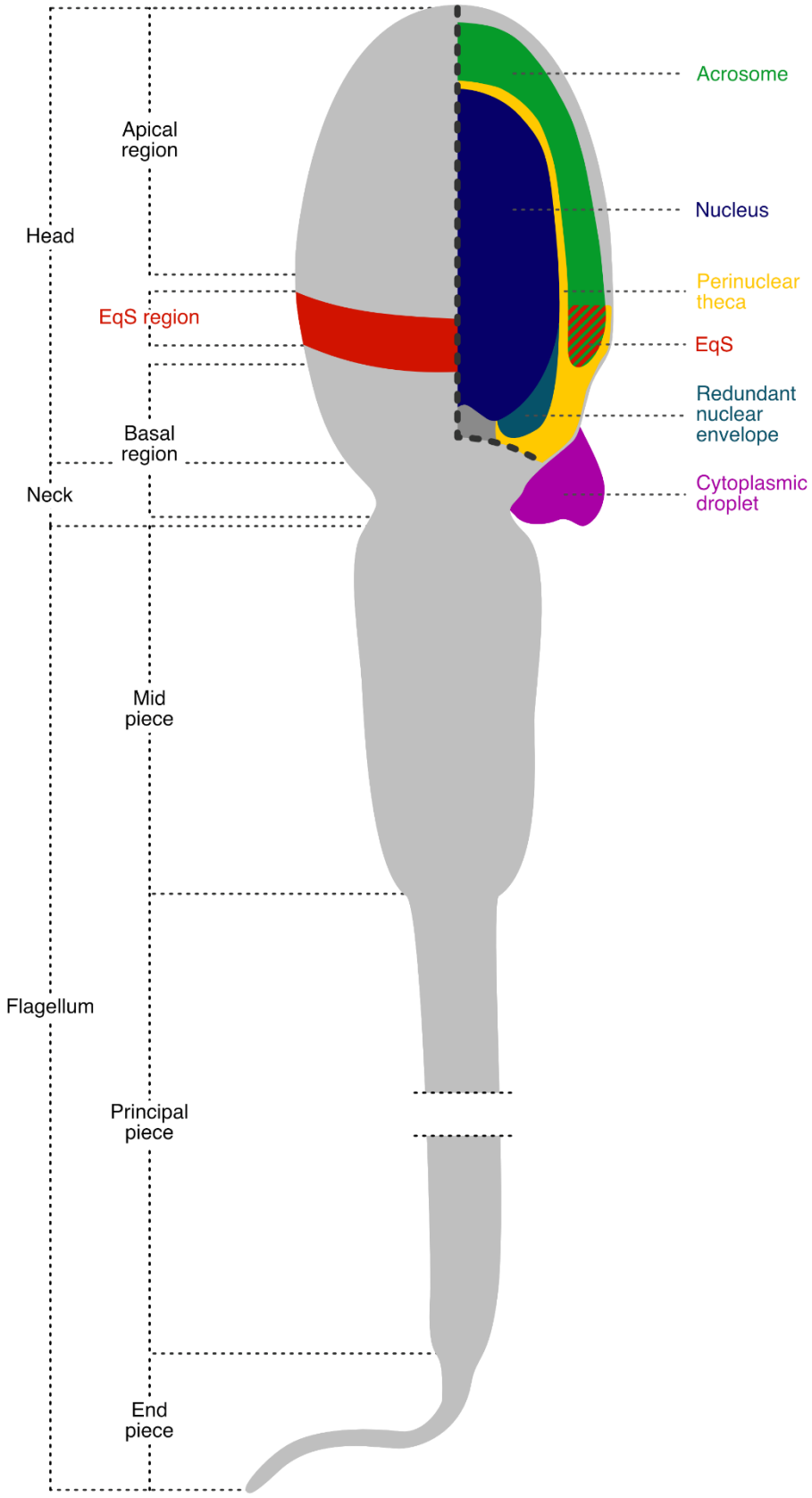


Supplementary figure 1: Schematic illustration of a human sperm illustrating the regions of interest mentioned in this article. EqS: Equatorial Segment, a subregion of the acrosome. EqS region: region of the sperm head (including the plasma membrane and the perinuclear theca) comprising the EqS.

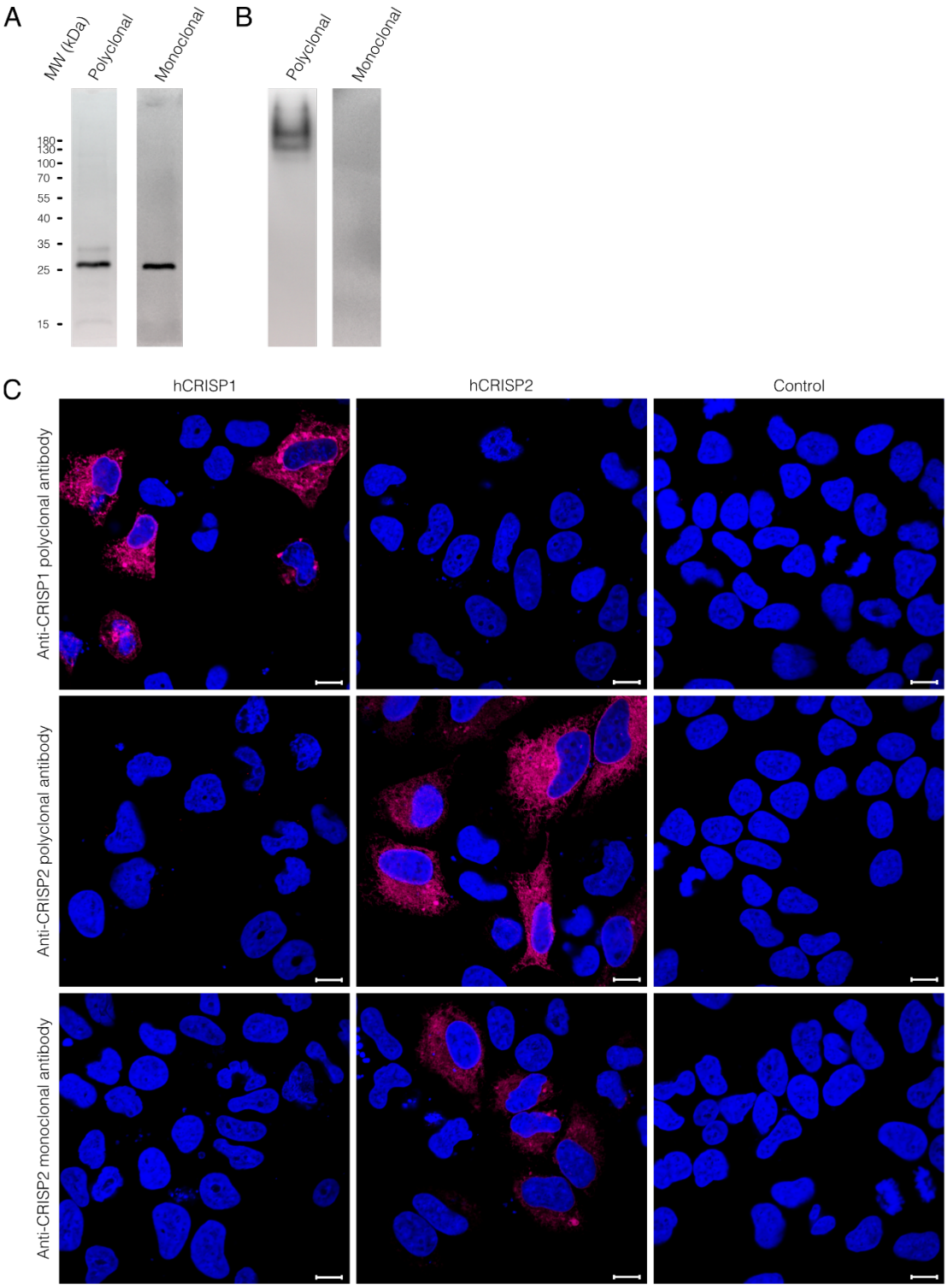


Supplementary Figure 2: Analysis of antibody specificity. Purified human sperm were extracted with PBS and proteins were resolved by A) SDS-PAGE (12% acrylamide) or B) Native-PAGE (10% acrylamide) and analyzed by western blot using rabbit polyclonal anti-hCRISP2 (Proteintech, Cat# 19066-1-AP) (Polyclonal) or mouse monoclonal anti-hCRISP2 (D-10) (Santa Cruz Biotechnology, Cat# sc-390914) (Monoclonal). C) HeLa cells transfected with expression vectors encoding for hCRISP1 and hCRISP2, or water (as a control) were analyzed in immunofluorescence using rabbit polyclonal anti-hCRISP1 (Sigma-Aldrich, Cat# HPA028445) and both anti-hCRISP2 antibodies. Magenta: hCRISP1 or hCRISP2. Blue: Hoechst staining of the nucleus. Scale bar: 10 µm. Images are equatorial views of the cells obtained from z stack images using Nikon NIS Elements software.

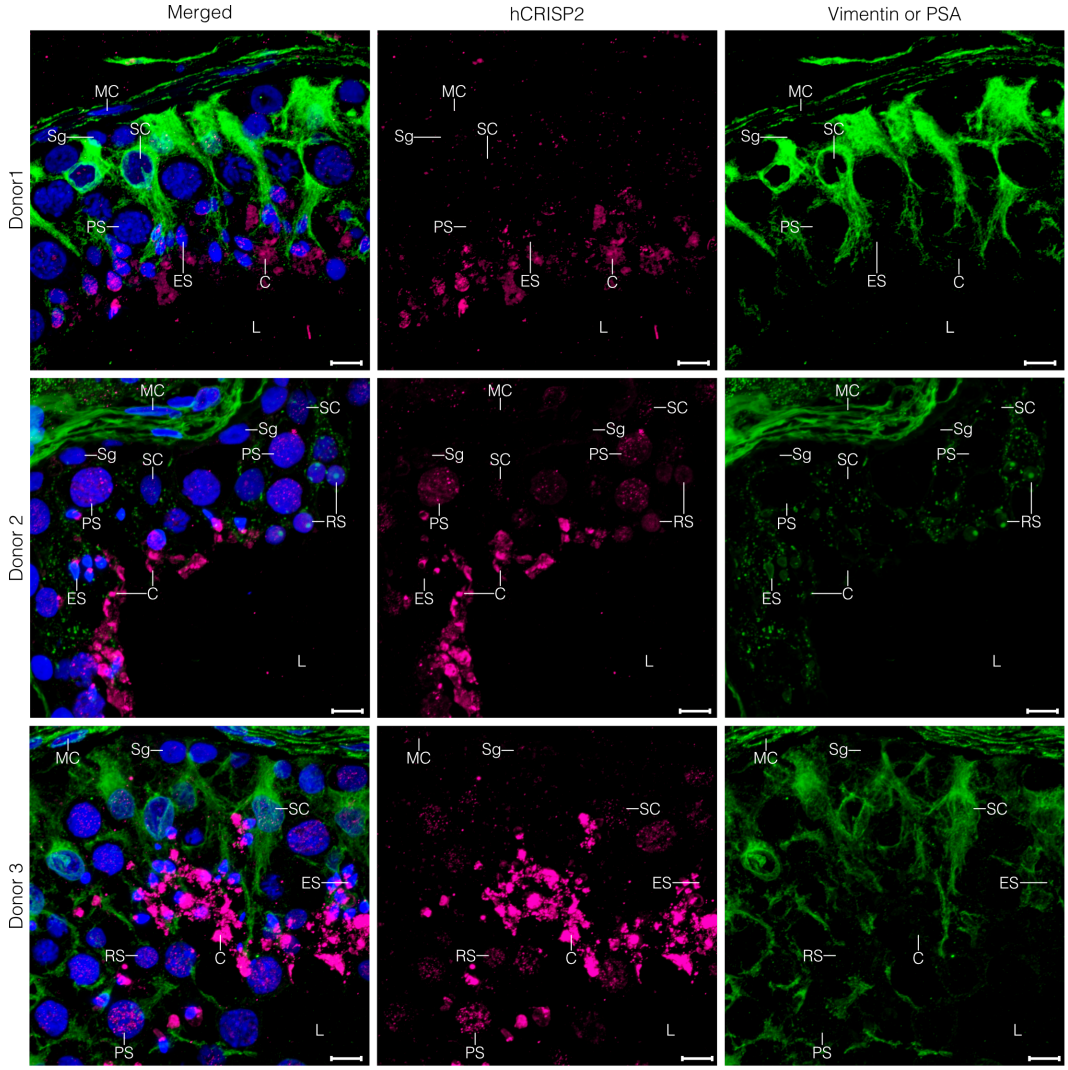


Supplementary Figure 3: Localization of CRISP2 on human testis sections in three different donors. Images are maximum-intensity projections (MaxIP) obtained from z stack images using Nikon NIS Elements software. Magenta: hCRISP2. Blue: Hoechst staining of the nucleus. Green: vimentin (used to highlight Sertoli Cells, in Donors 1 and 3) or PSA-FITC staining (used to visualize sperm acrosomes, in Donor 2). Scale bar: 10 µm. C, Cytoplasm; ES, Elongated Spermatid; L, Lumen of the seminiferous tubule; MC, Myoid Cell; PS, Primary Spermatocyte; RS, Round Spermatid; SC, Sertoli Cell; Sg, Spermatogonia.

.

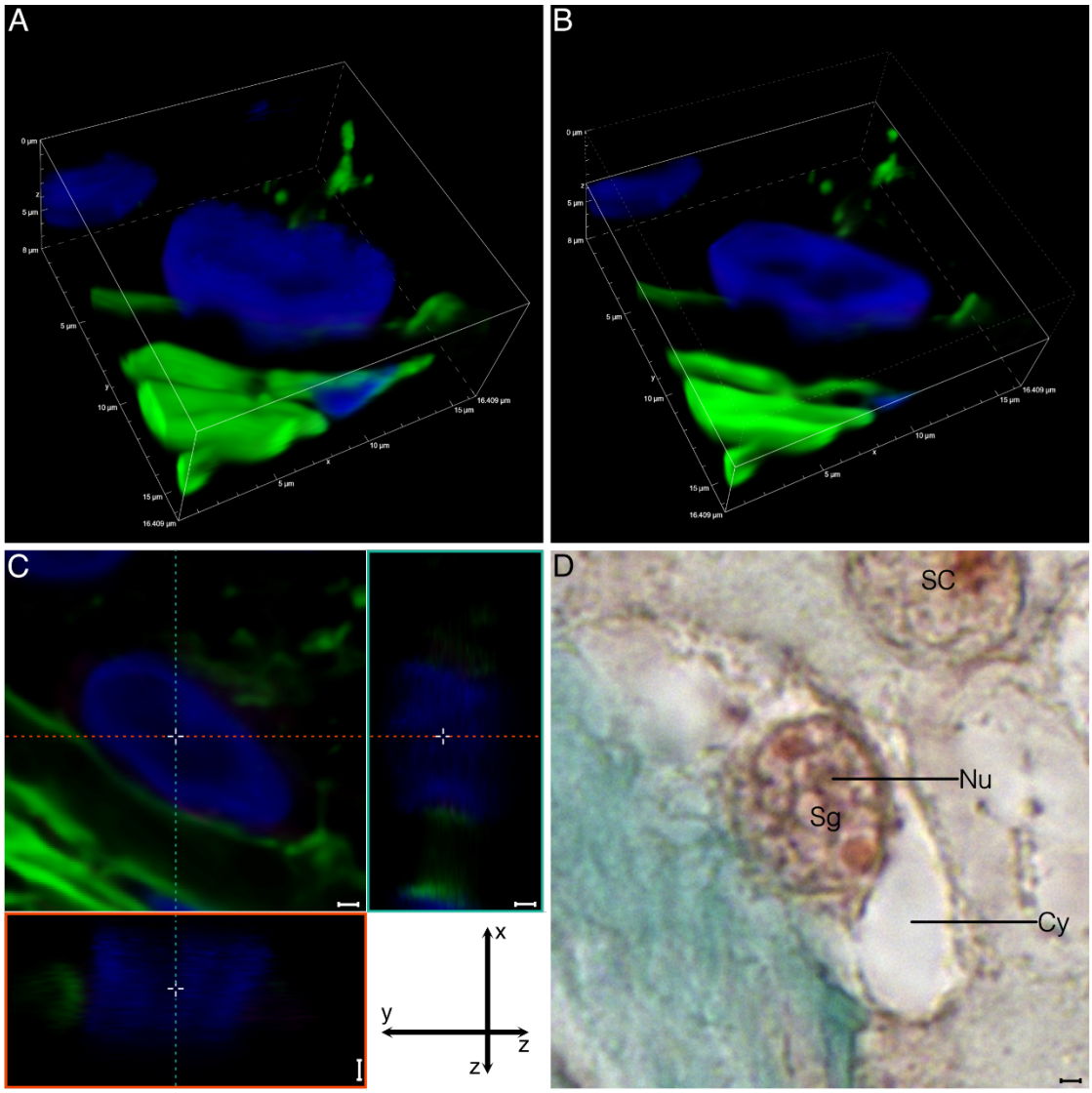


Supplementary Figure 4: Absence of hCRISP2 within a spermatogonium. (A,B) 3D rendered confocal z-stacks obtained using Nikon NIS Elements software. Full rendering is shown in panel A. For better clarity, partial rendering with orthogonal planar sectioning applied along the z-axis, leaving the hCRISP2 channel unaffected, is shown in panel B. The scale is shown on the edge of the box enclosing the spermatogonium. (C) Three orthogonal slice views (xy, xz, and yz planes), all intersecting at the empty cross marked point, providing detailed cross-sectional perspectives of the structure within the nucleus from different axes. No immunoreactivity was observed for hCRISP2 (in Magenta). Blue: Hoechst staining of the nucleus. Green: PSA-FITC staining (used to visualize sperm acrosomes). (D) Spermatogonium on a Masson's trichrome-stained testis section. Scale bar: 1 µm (C and D). Cy, Cytoplasm; Nu, Nucleus; SC, Sertoli Cell; Sg, Spermatogonium.

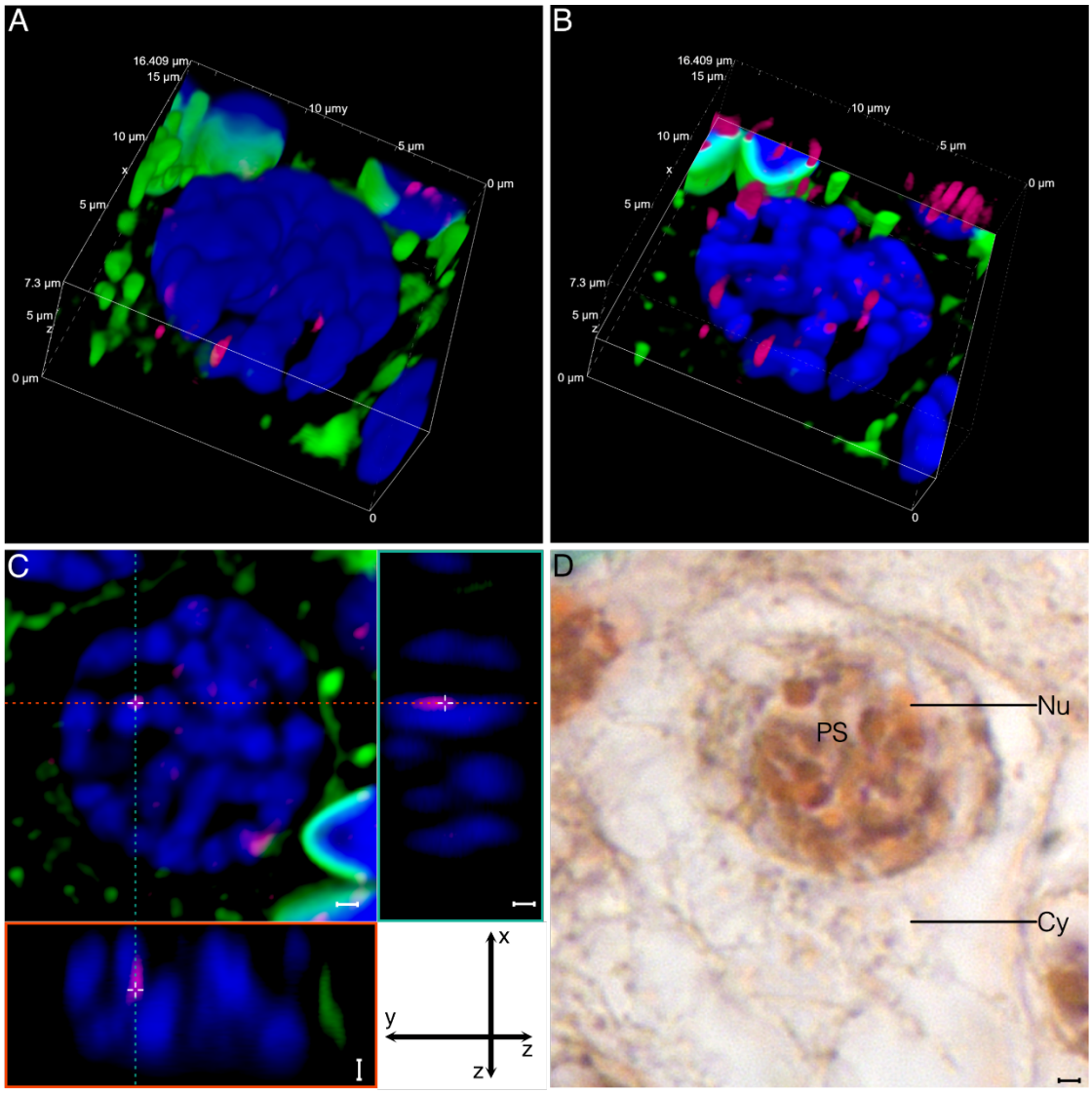


Supplementary Figure 5: Localization of hCRISP2 within a primary spermatocyte. (A,B) 3D rendered confocal z-stacks obtained using Nikon NIS Elements software. Full rendering is shown in panel A. For better clarity, partial rendering with orthogonal planar sectioning applied along the z-axis, leaving the hCRISP2 channel unaffected, is shown in panel B. The scale is shown on the edge of the box enclosing the primary spermatocyte. (C) Three orthogonal slice views (xy, xz, and yz planes), all intersecting at the empty cross marked point, providing detailed cross-sectional perspectives of the structure within the nucleus from different axes. Magenta: hCRISP2. Blue: Hoechst staining of the nucleus. Green: PSA-FITC staining (used to visualize sperm acrosomes). (D) Primary spermatocyte on a Masson's trichrome-stained testis section. Scale bar: 1 µm (C and D). Cy, Cytoplasm; Nu, Nucleus; PS: Primary Spermatocyte.

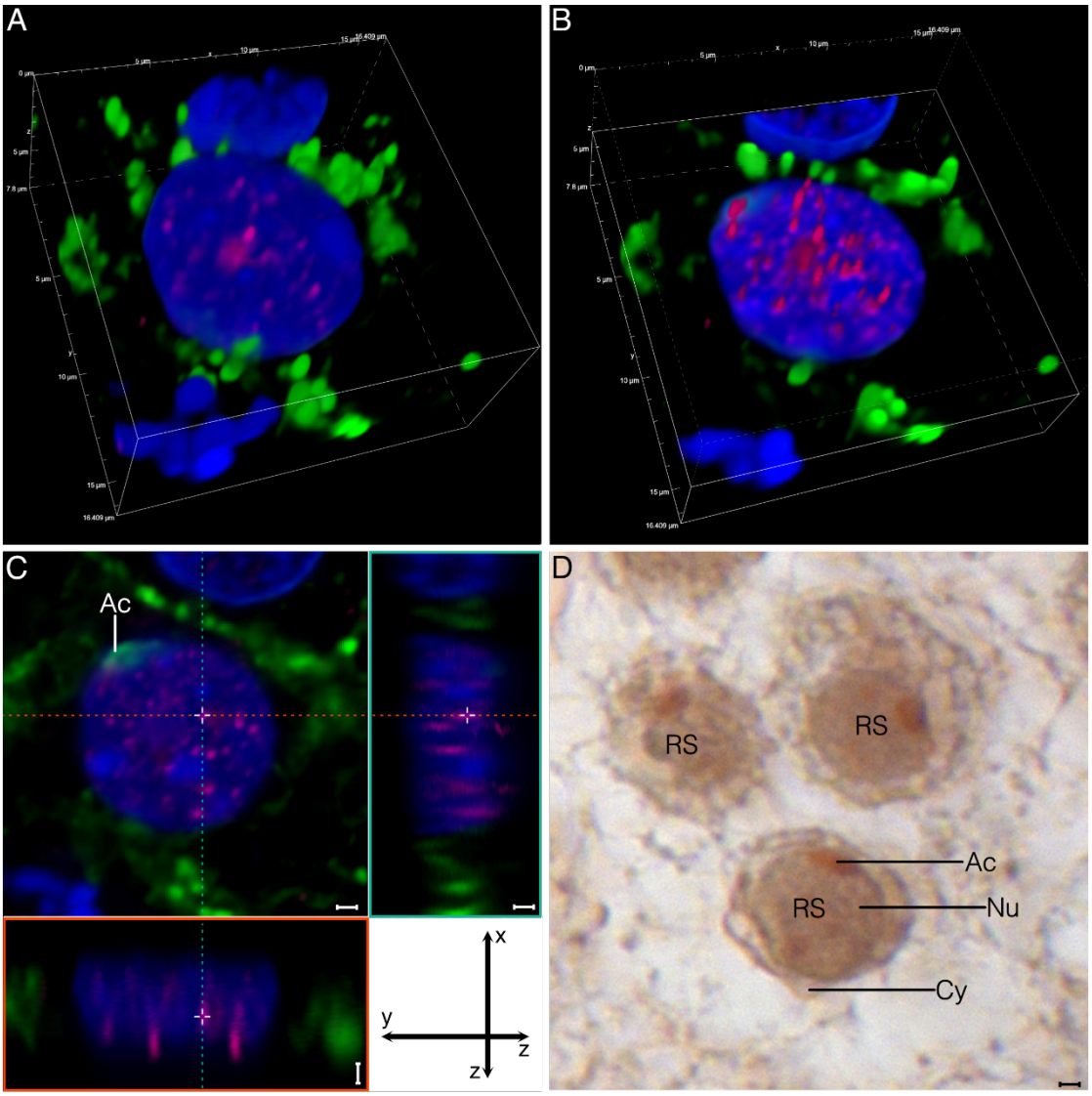


Supplementary Figure 6: Localization of hCRISP2 within an early round spermatid. (A,B) 3D rendered confocal z-stacks obtained using Nikon NIS Elements software. Full rendering is shown in panel A. For better clarity, partial rendering with orthogonal planar sectioning applied along the z-axis, leaving the hCRISP2 channel unaffected, is shown in panel B. The scale is shown on the edge of the box enclosing the early round spermatid. (C) Three orthogonal slice views (xy, xz, and yz planes), all intersecting at the empty cross marked point, providing detailed cross-sectional perspectives of the structure within the nucleus from different axes. Magenta: hCRISP2. Blue: Hoechst staining of the nucleus. Green: PSA-FITC staining (used to visualize sperm acrosomes). (D) Early round spermatid on a Masson's trichrome-stained testis section. Scale bar: 1 µm (C and D). Ac, Acrosome; Cy, Cytoplasm; Nu, Nucleus; RS, Round Spermatid.

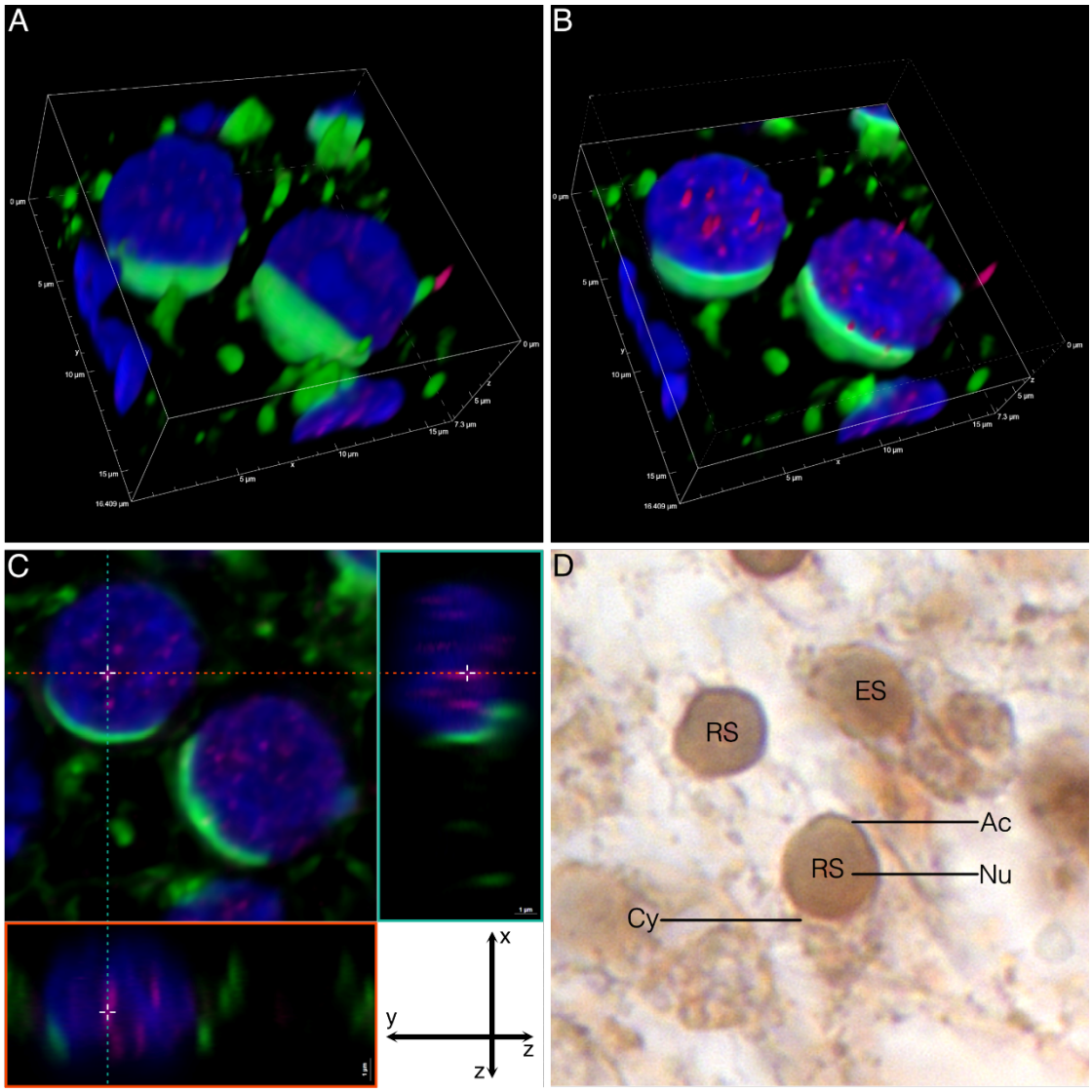


Supplementary Figure 7: Localization of hCRISP2 within a late round spermatid. (A,B) 3D rendered confocal z-stacks obtained using Nikon NIS Elements software. Full rendering is shown in panel A. For better clarity, partial rendering with orthogonal planar sectioning applied along the z-axis, leaving the hCRISP2 channel unaffected, is shown in panel B. The scale is shown on the edge of the box enclosing the late round spermatid. (C) Three orthogonal slice views (xy, xz, and yz planes), all intersecting at the empty cross marked point, providing detailed cross-sectional perspectives of the structure within the nucleus from different axes. Magenta: hCRISP2. Blue: Hoechst staining of the nucleus. Green: PSA-FITC staining (used to visualize sperm acrosomes). (D) Late round spermatid on a Masson's trichrome-stained testis section. Scale bar: 1 µm (C and D). Ac, Acrosome; Cy, Cytoplasm; ES, Elongated Spermatid; Nu, Nucleus; RS, Round Spermatid.

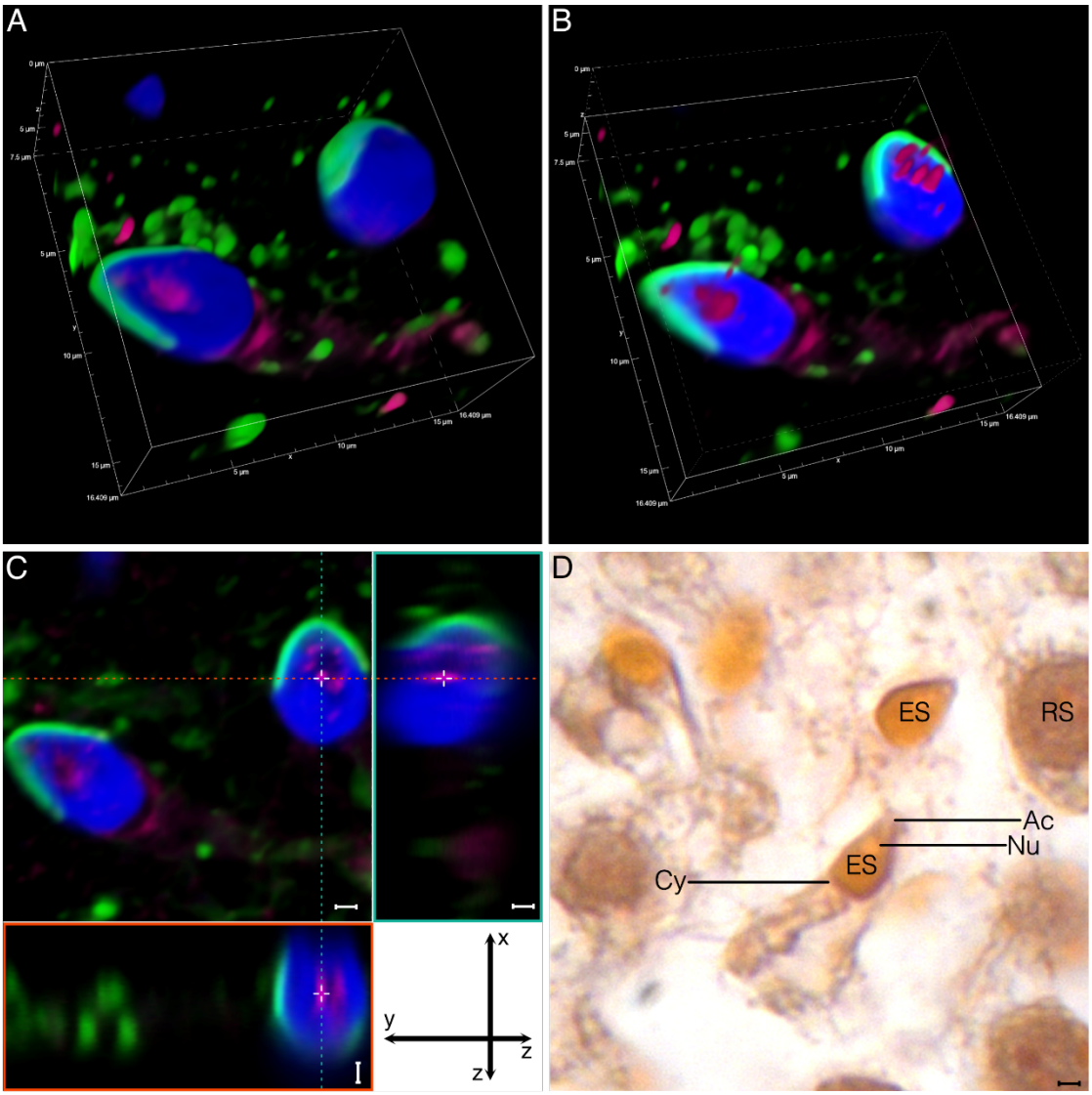


Supplementary Figure 8: Localization of hCRISP2 within an early elongated spermatid. (A,B) 3D rendered confocal z-stacks obtained using Nikon NIS Elements software. Full rendering is shown in panel A. For better clarity, partial rendering with orthogonal planar sectioning applied along the z-axis, leaving the hCRISP2 channel unaffected, is shown in panel B. The scale is shown on the edge of the box enclosing the early elongated spermatid. (C) Three orthogonal slice views (xy, xz, and yz planes), all intersecting at the empty cross marked point, providing detailed cross-sectional perspectives of the structure within the nucleus from different axes. Magenta: hCRISP2. Blue: Hoechst staining of the nucleus. Green: PSA-FITC staining (used to visualize sperm acrosomes). (D) Early elongated spermatid on a Masson's trichrome-stained testis section. Scale bar: 1 µm (C and D). Ac, Acrosome; Cy, Cytoplasm; ES, Elongated Spermatid; Nu, Nucleus; RS, Round Spermatid.

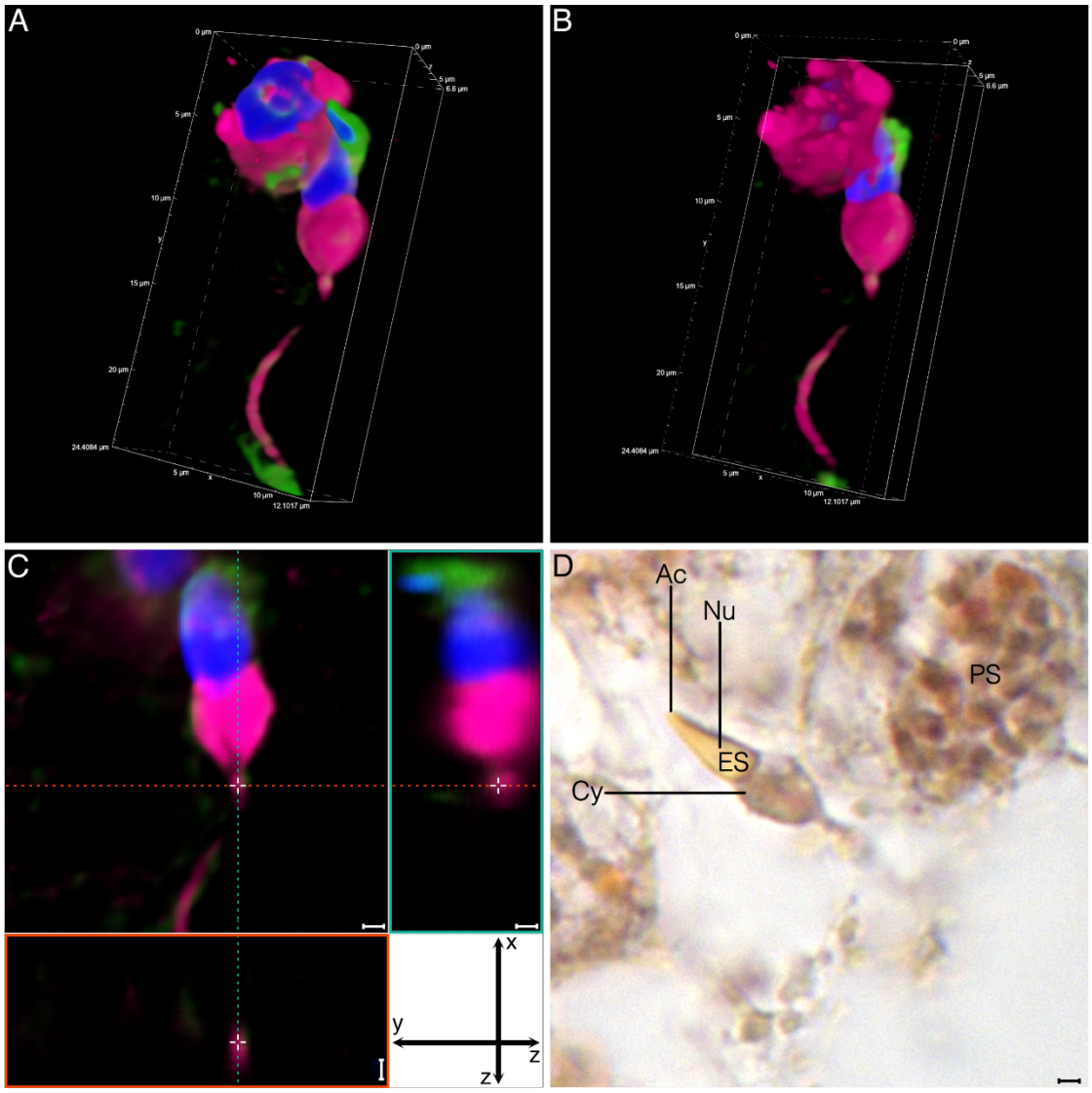


Supplementary Figure 9: Localization of hCRISP2 within a late elongated spermatid. (A,B) 3D rendered confocal z-stacks obtained using Nikon NIS Elements software. Full rendering is shown in panel A. For better clarity, partial rendering with orthogonal planar sectioning applied along the z-axis, leaving the hCRISP2 channel unaffected, is shown in panel B. The scale is shown on the edge of the box enclosing the late elongated spermatid. (C) Three orthogonal slice views (xy, xz, and yz planes), all intersecting at the empty cross marked point, providing detailed cross-sectional perspectives of the structure within the nucleus from different axes. Magenta: hCRISP2. Blue: Hoechst staining of the nucleus. Green: PSA-FITC staining (used to visualize sperm acrosomes). (D) Late elongated spermatid on a Masson's trichrome-stained testis section. Scale bar: 1 µm (C and D). Ac, Acrosome; Cy, Cytoplasm; ES, Elongated Spermatid; Nu, Nucleus; PS, Primary Spermatocyte.

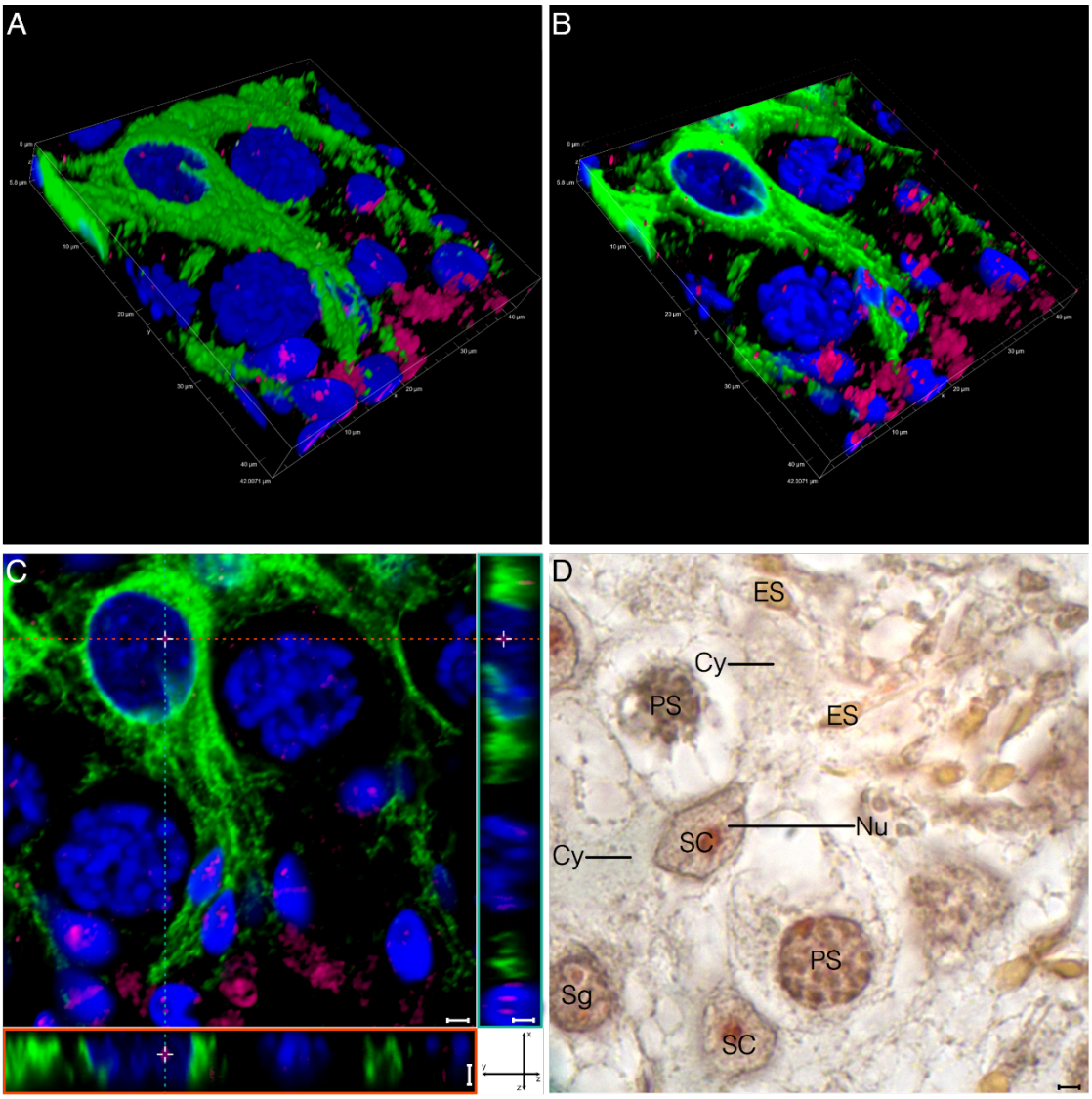


Supplementary Figure 10: Localization of hCRISP2 within a Sertoli cell. (A,B) 3D rendered confocal z-stacks obtained using Nikon NIS Elements software. Full rendering is shown in panel A. For better clarity, partial rendering with orthogonal planar sectioning applied along the z-axis, leaving the hCRISP2 channel unaffected, is shown in panel B. The scale is shown on the edge of the box enclosing the Sertoli cell. (C) Three orthogonal slice views (xy, xz, and yz planes), all intersecting at the empty cross marked point, providing detailed cross-sectional perspectives of the structure within the nucleus from different axes. Magenta: hCRISP2. Blue: Hoechst staining of the nucleus. Green: PSA-FITC staining (used to visualize sperm acrosomes). (D) Sertoli cell on a Masson's trichrome-stained testis section. Scale bar: 1 µm (C and D). Cy, Cytoplasm; ES, Elongated Spermatid; Nu, Nucleus; PS, Primary Spermatocyte; SC, Sertoli's Cell; Sg, Spermatogonium.

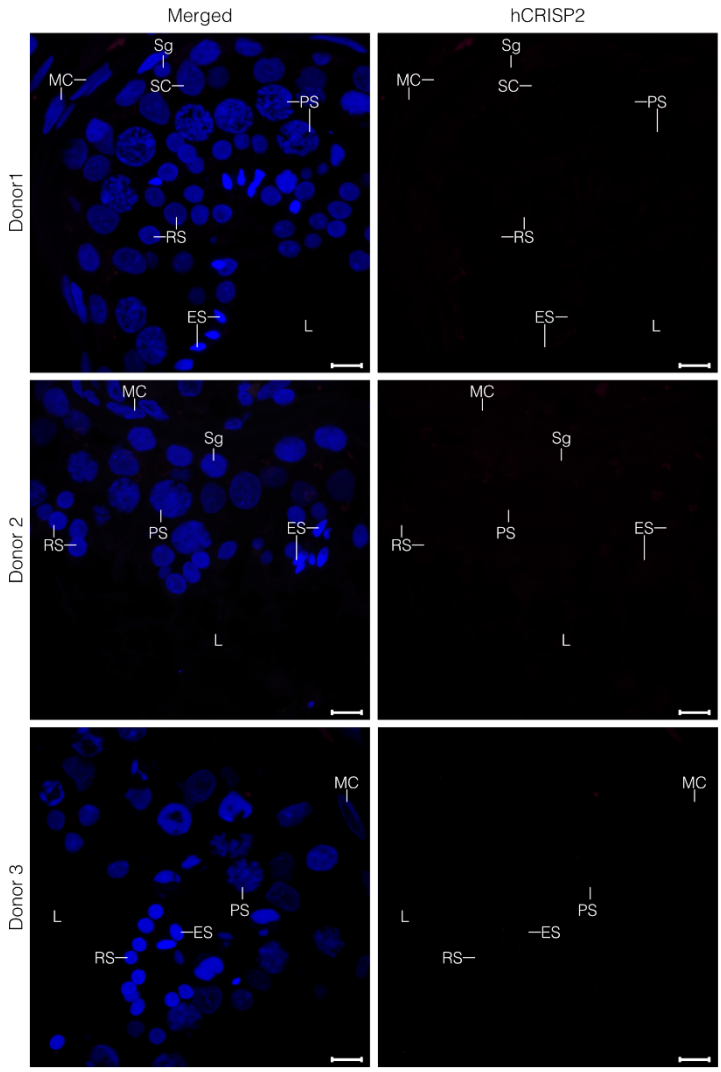


Supplementary Figure 11: Control for the immunostaining of CRISP2 in human testis, in which incubation with primary antibody was omitted. Images are maximum-intensity projections (MaxIP) obtained from z stack images using Nikon NIS Elements software. No immunoreactivity was observed for hCRISP2 (in Magenta). Blue: Hoechst staining of the nucleus. Scale bar: 10 µm. ES, Elongated spermatid; L, lumen of the seminiferous tubule; MC, myoid cell; PS, Primary Spermatocyte; RS, Round Spermatid; SC, Sertoli Cell; Sg, Spermatogonium.

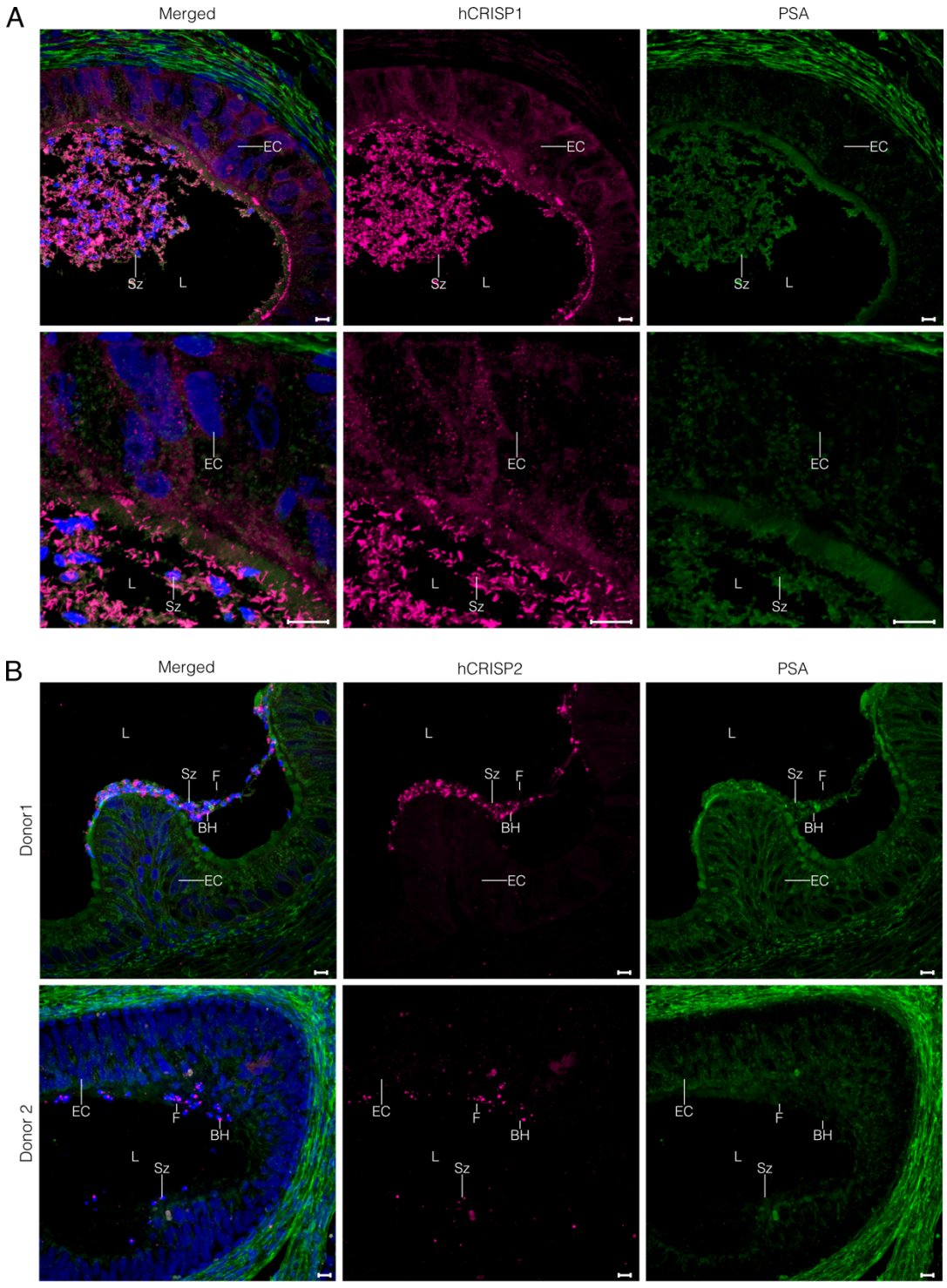


Supplementary Figure 12: continues on the next page.

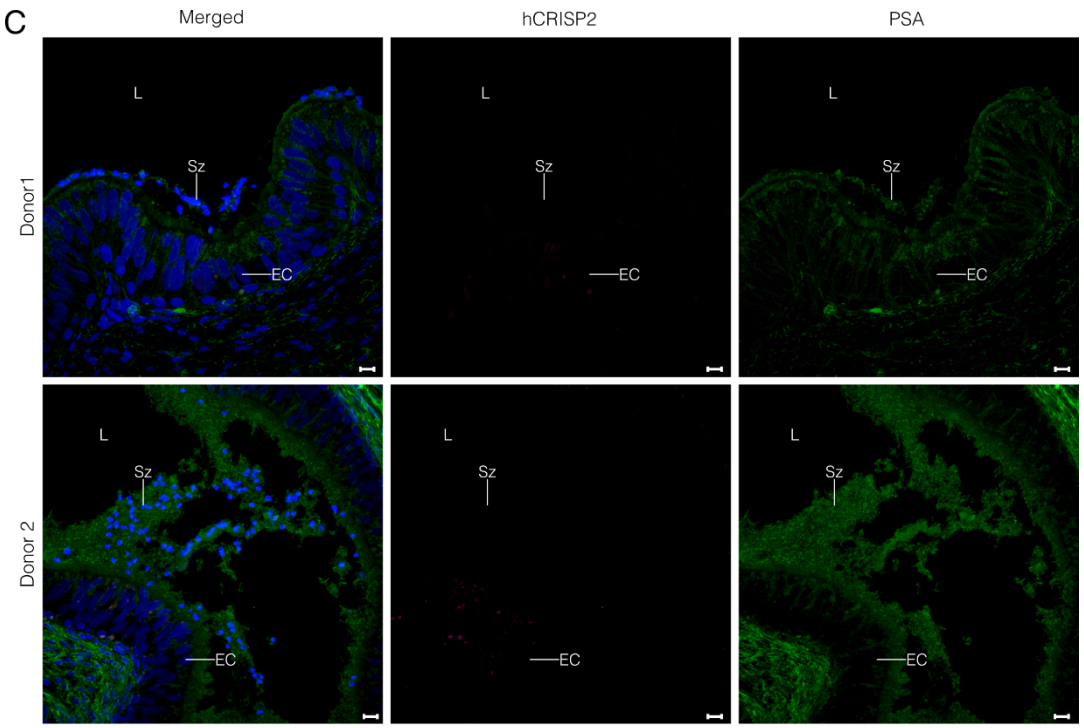


Supplementary Figure 12: Localization of hCRISP1 and hCRISP2 on human epididymis sections from two donors. A) hCRISP1 localization from donor 1. Scale bar: 10 µm. B) General view of hCRISP2 immunostaining provided in Fig. 3 (top) and from donor 2 (bottom). Scale bar: 20 µm C) Controls, in which incubation with primary antibody was omitted, no immunoreactivity was observed for hCRISP2. Scale bar: 10 µm. Images are maximum-intensity projections (MaxIP) obtained from z stack images using Nikon NIS Elements software. Magenta: hCRISP1 or hCRISP2. Blue: Hoechst staining of the nucleus. Green: PSA-FITC staining (used to visualize sperm acrosomes). Scale bar: 10 µm. BH, Basal region of the Head; EC, Epithelial Cell; F, Flagellum; L, Lumen of the epididymis; Sz, Sperm.

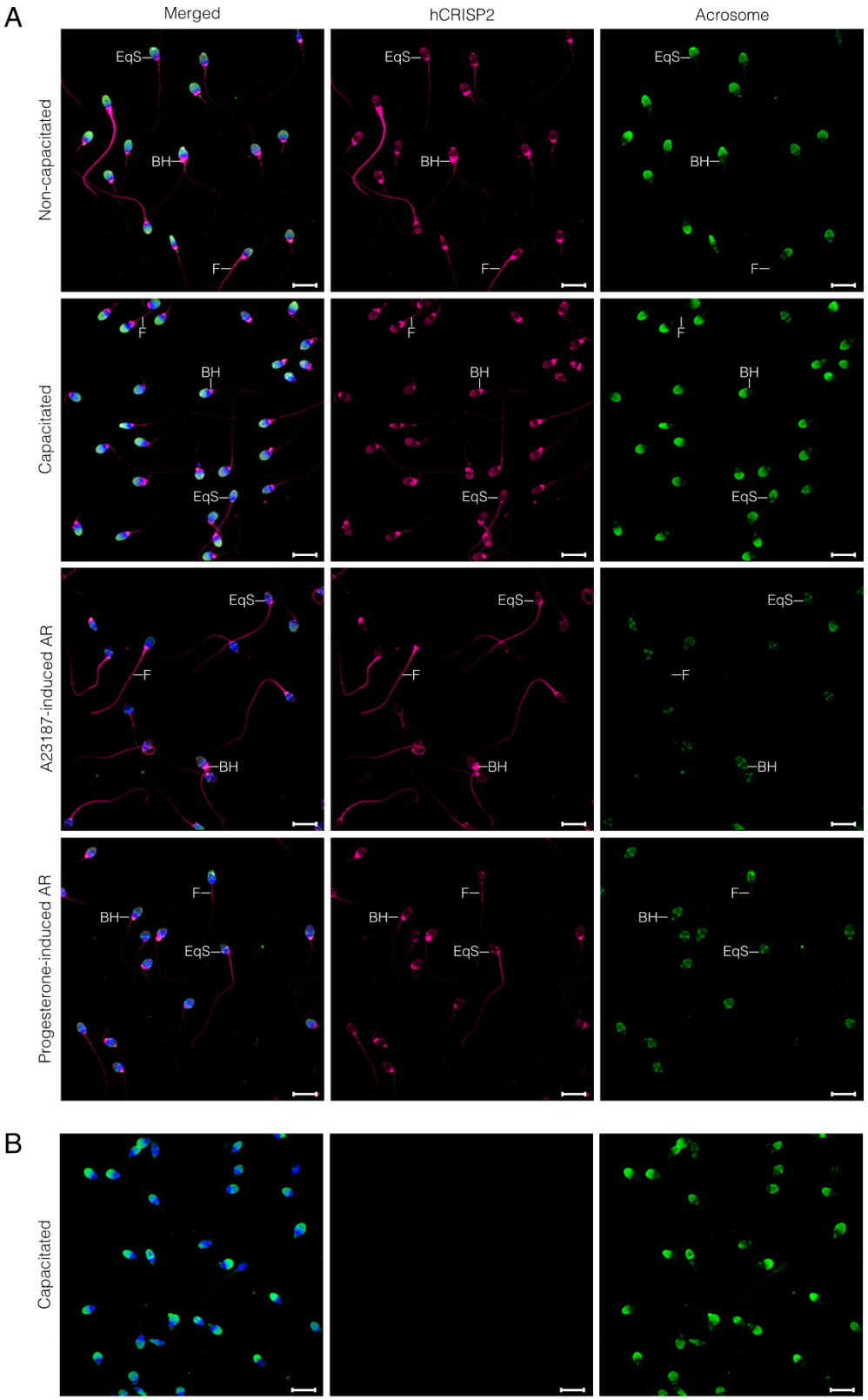


Supplementary Figure 13: General views (A) and control (B) for the immunostaining of hCRISP2 on ejaculated human sperm before and after capacitation as well as after acrosomal reaction (AR) induced either by calcium ionophore (A23187) or progesterone. Images are maximum-intensity projections (MaxIP) obtained from z stack images using Nikon NIS Elements software. Magenta: hCRISP2. Blue: DAPI staining of the nucleus. Green: PSA-FITC staining (used to visualize sperm acrosomes). Scale bar: 10 µm. BH, Basal region of the Head; EqS, Equatorial Segment; F, Flagellum. Representative results from N = 3 replicates.

A

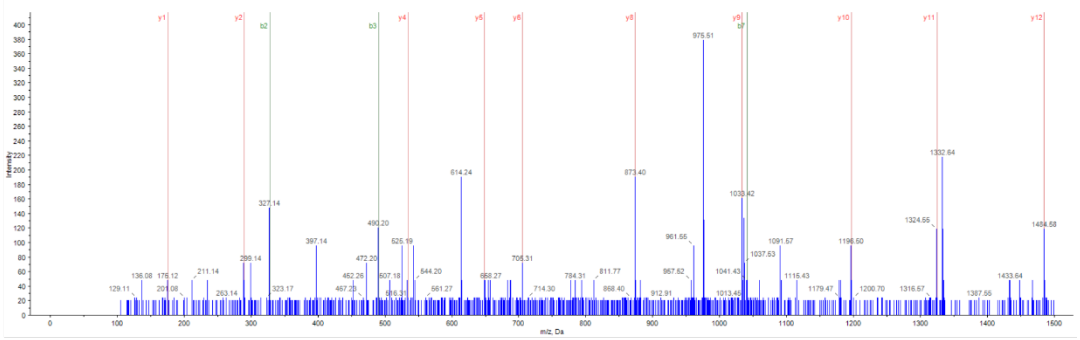


B

| Residue | b | b+2 | y | y+2 |
|---|---|---|---|---|
| Y | 164.0706 | 82.5389 | 2072.8412 | 1036.9242 |
| Y | **327.1339** | 164.0706 | 1909.7778 | 955.3926 |
| Y | **490.1973** | 245.6023 | 1746.7145 | 873.8609 |
| V | 589.2657 | 295.1365 | 1583.6512 | 792.3292 |
| C[CAM] | 749.2963 | 375.1518 | **1484.5828** | 742.7950 |
| Q | 877.3549 | 439.1811 | **1324.5521** | 662.7797 |
| Y | **1040.4182** | 520.7128 | **1196.4935** | 598.7504 |
| C[CAM] | 1200.4489 | 600.7281 | **1033.4302** | 517.2187 |
| P | 1297.5016 | 649.2545 | **873.3996** | 437.2034 |
| A | 1368.5388 | 684.7730 | 776.3468 | 388.6770 |
| G | 1425.5602 | 713.2837 | **705.3097** | 353.1585 |
| N | 1539.6031 | 770.3052 | **648.2682** | 324.6477 |
| N | 1653.6461 | 827.3267 | **534.2453** | 267.6263 |
| M | 1784.6866 | 892.8469 | 420.2024 | 210.6048 |
| N | 1898.7295 | 949.8684 | **289.1619** | 145.0846 |
| R | 2054.8306 | 1027.9189 | **175.1190** | 88.0631 |

Supplementary Figure 14: Mass spectrometry analysis of the discriminant peptide specific to the shorter hCRISP2 isoform (P16562-1). A) Fragmentation spectrum of YYYVCQYCPAGNNMNR peptide from hCRISP2. B) Fragment ions table from the fragmentation spectrum. Cells highlighted in green indicate the detected ions. Spectrum and table were obtained from ProteinPilot Software.

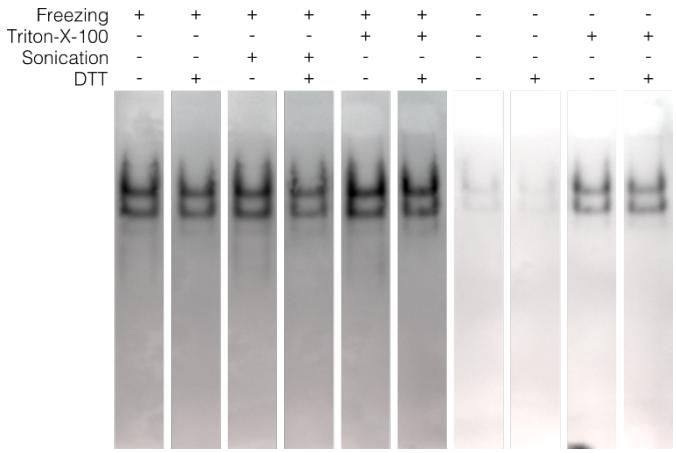


Supplementary Figure 15: Influence of different treatments on hCRISP2 electrophoretic mobility. Proteins were extracted from fresh or frozen purified sperm using PBS, in the presence or absence of Triton-X-100, with or without sonication, and resolved using Native-PAGE, with or without DTT in the loading buffer. They were then analyzed in western blot using polyclonal anti-hCRISP2. Results from frozen (left) and fresh (right) sperm originate from two different donors.

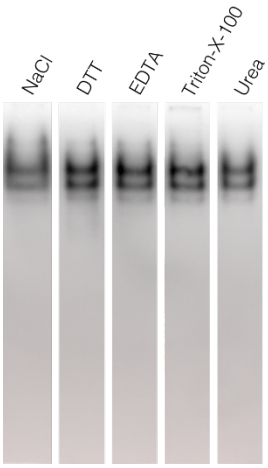


Supplementary Figure 16: Influence of different agents on the electrophoretic pattern of hCRISP2. Proteins were extracted from purified sperm using PBS, and incubated in the presence of either 1 M NaCl to disrupt ionic bounds, 100 mM DTT to disrupt disulfide bounds, 24 mM EDTA to chelate metallic ions, 1 % Triton-X-100 to disrupt hydrophobic interactions, or 4 M urea to disrupt hydrogen bounds and hydrophobic interactions. Samples were then resolved by Native-PAGE (10% acrylamide) and analyzed in western blot using polyclonal anti-hCRISP2. Representative results from N = 3 replicates.

Supplementary Table 1: Literature review of studies addressing the localization of CRISP2 in mammals on testis sections or sperm.

| Reference | Species | Experiment | Antibody used | Localization | |
|---|---|---|---|---|---|
| (Hardy et al. 1988) | Guinea pig | IIF on epididymal sperm | Homemade, obtained by immunization of guinea pigs or rabbits with purified AA1 | Labeling in the acrosomal region | |
| | | IIF on testicular cells smear | | PS | Small granules in the perinuclear region (probably Golgi) |
| | | | | SS | Coarser granules |
| | | | | RS | Round granules |
| | | | | ES | Acrosomal labeling |
| | | | | Sz | |
| (Maeda et al. 1998) | Rat (Donryu) | IHC on cultured spermatic cells | Homemade, obtained by immunization of rabbits with recombinant TPX-1 (aa 89-243) | Most cells are labelled | |
| (Maeda et al. 1999) | Rat (Donryu) | IHC on testis sections | Homemade, obtained by immunization of rabbits with synthetic peptide of TPX-1 (aa 23-40) | PS | Weak labeling |
| | | | | SS | |
| | | | | RS | |
| | | | | ES | Intense labeling |
| (Kim et al. 2001) | Guinea pig | IIF on epididymal sperm | Homemade rabbit polyclonal (same as (Hardy et al. 1988)) | Before AR | Strong labeling in the acrosomal part |
| | | | | After AR | No labeling in the acrosomal part |
| (O'Bryan et al. 2001) | Rat (Sprague-Dawley) | IHC on testis sections | Homemade, obtained by immunization of rabbits with synthetic peptides of TPX-1 (aa 34-49; 182-191; 222-236) | PS | No labeling |
| | | | | SS | |
| | | | | RS | Labeling in the developing acrosome region |
| | | | | ES | Labeling in the perforatorium, the cytoplasmic lobe ("granulated bodies"), the developing flagellum and, at the end of spermiogenesis, flagellum principal piece. |
| | | | | SC | Labeling in the residual bodies (from the phagocytosis of "granulated bodies") |
| | | Immuno-TEM on testis sections | | RS | Labeling in the acrosome |
| | | | | ES | Labeling in the acrosome, the ODF of principal and intermediate piece, the fibrous column of longitudinal sheets, and connecting piece |
| | | | | SC | No noticeable labeling |
| (Busso et al. 2005) | Human | IIF on ejaculated sperm | Homemade, obtained by immunization of rabbits with recombinant TPX-1 fused with MBP | Before Capa | Before permeabilization: no or very weak labeling of the acrosome.<br>After permeabilization: strong labeling in the acrosome and weak labeling in the neck and flagellum |
| | | | | After Capa | Strong labeling in the acrosome and weak labeling in the neck and flagellum |

| | | | | | |
|---|---|---|---|---|---|
| | | | | After AR | Labeling at the EqS or very weak in the acrosomal part |
| (Du et al. 2006) | Human | IHC on testis sections | Homemade, obtained by immunization of mice with recombinant TPX-1 fused with His-Tag | Sg | No labeling |
| | | | | PS | Strong cytoplasmic and cytoplasmic membrane labeling |
| | | | | ES | Weak cytoplasmic and cytoplasmic membrane labeling |
| | | | | SC | No labeling |
| | | | | LC | No labeling |
| | | IIF on ejaculated sperm | | Labeling as dense spot at the connecting piece, weak labeling in the flagellum and acrosome | |
| (Busso et al. 2007) | Mouse (CF1) | IIF on epididymal sperm | Homemade, obtained by immunization of rabbits with recombinant hCRISP2 | Before Capa | Paraformaldehyde fixed sperm: weak labeling in the acrosomal region<br>Acetone fixed or MeOH permeabilized sperm: strong labeling in the dorsal region of the acrosome and weak labeling in the principal piece of the flagellum |
| | | | | After Capa | |
| | | | | After AR | Strong labeling at the tip of the acrosome |
| (Gibbs et al. 2007) | Mouse (CBA x C57BI6) | IIF on epididymal sperm | Homemade (same as (O'Bryan et al. 2001)) | Labeling in the acrosome and in the intermediate and principal pieces of the flagellum | |
| (Jamsai et al. 2008a) | Mouse | IIF on epididymal sperm | Mouse monoclonal anti-CRISP2 (R&D Systems, Minneapolis, MN, USA Cat# MAB2575) | Labeling in the acrosome and in the principal piece of the flagellum | |
| (Jamsai et al. 2008b) | Human | IHC on testis sections | Homemade (same as (O'Bryan et al. 2001)) | RS | Labeling in the developing and mature acrosome and flagellum |
| | | | | ES | |
| (Jamsai et al. 2009) | Mouse | IIF on epididymal sperm | Mouse monoclonal anti-CRISP2 (R&D Systems, Minneapolis, MN, USA Cat# MAB2575) | Labeling in the sperm head and in the principal and intermediate pieces of the flagellum | |
| (Munoz et al. 2012) | Rat (Wistar) | IIF on epididymal sperm | Homemade, obtained by immunization of rats with recombinant CRISP2 fused with MBP | Before Capa | Before permeabilization: no or very weak labeling of the acrosome.<br>After permeabilization: labeling in the dorsal region of the acrosome along with concave region of the sperm head or only in the concave region |
| | | | | After Capa | Mostly labeling only in the concave region of the sperm head |
| | | | | After AR | |
| (Nimlamool et al. 2013) | Human | IIF on ejaculated sperm | Rabbit polyclonal anti-hCRISP2 (Sigma-Aldrich, St Louis, MO, USA Cat# non specified) | Before Capa | Before permeabilization: no labeling.<br>After permeabilization: strong labeling in the anterior part of the acrosome and in the neck |
| | | | | After Capa | Strong labeling in the anterior part of the acrosome and in the neck |

| | | | | | |
|---|---|---|---|---|---|
| | | | | After AR | No labeling in the anterior part of the acrosome and labeling at the EqS |
| (Anklesaria et al. 2016) | Human | IIF on ejaculated sperm | Homemade, obtained by immunization of rabbits with synthetic peptide of CRISP2 (aa 219-231) | Labeling in the connecting and principal pieces of the flagellum | |
| (Gao et al. 2021) | Verrat (Yorkshire) | IHC on testis sections | Goat polyclonal anti-CRISP2 (Sigma-Aldrich, St Louis, MO, USA Cat# SAB2501635) | Sg | Labeling in the cytoplasm |
| | | | | PS | |
| | | | | SS | |
| | | | | RS | |
| | | | | ES | |
| | | IIF on ejaculated sperm | | Before Capa | Labeling in the post-acrosomal region of the sperm head, the neck, and the flagellum |
| | | | | After Capa | Labeling in the apical segment and the post acrosomal region of the sperm head and the intermediate piece |
| (Zhang et al. 2021) | Verrat | IIF on ejaculated sperm | Rabbit polyclonal anti-CRISP2 (Proteintech, Manchester, GBR Cat# 19066–1-A)<br>Goat polyclonal anti-CRISP2 (MyBiosource, San Diego, CA, USA Cat# MBS422304) | Before Capa | Before permeabilization: labeling at the limit between the post-acrosomal region and the EqS<br>After permeabilization: weak labeling in the acrosome, the neck, and the intermediate and mid parts of the principal piece |
| | | | | After Capa | Strong labeling in the post acrosomal region and connecting piece |
| | | Immuno-TEM on ejaculated sperm | | Labeling in the PT, ODF and fibrous column of longitudinal sheets of the principal piece | |
| (Wittayarat et al. 2021) | Malayan tapir | IIF on ejaculated sperm | Rabbit polyclonal anti-CRISP2 (Abcam, Amsterdam, NLD Cat# ab117442) | Before Capa | Labelling in the mid piece and the flagellum |
| (Zhang et al. 2022) | Verrat | IIF on ejaculated sperm | Goat polyclonal anti-CRISP2 (MyBiosource, San Diego, CA, USA Cat# MBS422304) | Before Capa | Strong labeling in the post-acrosomal region and connecting piece and a weak labeling in the flagellum<br>After permeabilization: labeling at the apical part of the sperm head |
| | | | | After Capa | Strong labeling in the post-acrosomal region and connecting piece and weak labeling in the flagellum or strong labeling at the EqS and the apical part of the sperm head |
| | | | | After AR | Labeling in an adjacent region of the EqS |
| (Wittayarat et al. 2024) | Fishing cat | IIF on ejaculated sperm | Rabbit polyclonal anti-CRISP2 (Abcam, Amsterdam, NLD Cat# ab117442) | Before Capa | Labeling in the whole sperm head |

AA, Amino Acids; AR, Acrosomal Reaction; Capa, Capacitation; EqS, Equatorial Segment; ES, Elongated Spermatid; IIF, Indirect Immunofluorescence; IHC, Immunohistochemistry; LC, Leydig Cell; MBP, Maltose Binding Protein; ODF, Outer Dense Fiber; PS, Primary Spermatocyte; PT, Perinuclear Theca; Sg, Spermatogonium; RS, Rond Spermatid; SS, Secondary Spermatocyte; SC, Sertoli Cell; Sz, Sperm; TEM, Transmission Electron Microscopy. AA1 (Autoantigen 1) and TPX1 (Testis-specific protein) are alias used to name CRISP2.

Supplementary Table 2: Mass spectrometry analysis of CRISP2 complexes immunoprecipitated from non-capacitated human sperm.

| Uniprot Accession Number | Gene Name | Protein name | Peptide number [a] | | | | | |
|---|---|---|---|---|---|---|---|---|
| | | | Experiment A | Experiment B | | Experiment C | | |
| | | | hCRISP2 | hCRISP2 | hHSP70 [b] | hCRISP2 | Rabbit IgG [b] | Dynabeads only [b] |
| P16562 | CRISP2 | Cysteine-rich secretory protein 2 | 12 | 21 | / | 16 | / | / |
| P54652 | HSPA2 | Heat shock-related 70 kDa protein 2 [c] | / | / | 6 | / | / | / |
| P34931 | HSPA1L | Heat shock 70 kDa protein 1-like [c] | / | / | 24 | / | / | / |
| P0DMV8 | HSPA1A | Heat shock 70 kDa protein 1A [c] | / | / | 18 | / | / | / |
| P10323 | ACR | Acrosin | 8 | 10 | 11 | 15 | 13 | 9 |
| Q8NEB7 | ACRBP | Acrosin-binding protein | 8 | 10 | 13 | 10 | 9 | 6 |
| P02768 | ALB | Albumin | / | / | 6 | / | / | / |
| P08118 | MSMB | Beta-microseminoprotein | / | / | / | 3 | / | / |
| P49913 | CAMP | Cathelicidin antimicrobial peptide | / | / | 2 | / | / | / |
| V9HW68 | HEL-214 | Epididymis luminal protein 214 [d] | 3 | 2 | / | / | / | / |
| Q9BTM1 | H2AJ | Histone H2A.J | / | / | / | 3 | 3 | 2 |
| Q99880 | H2BC13 | Histone H2B type 1-L | / | / | / | 2 | / | 2 |
| Q96RW9 | PLA2 | Mutant synovial phospholipase A2 (Fragment) [e] | / | / | 3 | / | 2 | / |
| P14555 | PLA2G2A | Phospholipase A2, membrane associated [e] | / | 4 | / | / | / | / |
| Q02383 | SEMG2 | Semenogelin-2 | / | / | 3 | / | 2 | 2 |
| P04279 | SEMG1 | Semenogelin-1 | / | / | 2 | / | / | / |

| | | | | | | | | |
|---|---|---|---|---|---|---|---|---|
| P20155 | SPINK2 | Serine protease inhibitor Kazal-type 2 | / | / | 2 | / | / | / |
| Q8WVW5 | / | Uncharacterized protein (Fragment) [f] | / | 6 | 6 | / | / | / |
| P81605 | DCD | Dermcidin | / | / | 2 | / | / | / |
| P07477 | PRSS1 | Serine protease 1 [g] | 3 | / | / | / | / | / |
| P04264 | KRT1 | Keratin, type II cytoskeletal 1 | 14 | 12 | 10 | 19 | 18 | 24 |
| P35908 | KRT2 | Keratin, type II cytoskeletal 2 epidermal | / | 11 | 2 | 13 | 10 | 3 |
| P13647 | KRT5 | Keratin, type II cytoskeletal 5 | / | / | / | 4 | 4 | 9 |
| P13647 | KRT5 | Keratin, type II cytoskeletal 5 | / | 2 | / | / | / | / |
| P02538 | KRT6A | Keratin, type II cytoskeletal 6A | / | / | / | / | 4 | / |
| P35527 | KRT9 | Keratin, type I cytoskeletal 9 | 11 | 10 | 9 | 10 | 15 | 21 |
| P13645 | KRT10 | Keratin, type I cytoskeletal 10 | 5 | 13 | 7 | 10 | 9 | 8 |
| P02533 | KRT14 | Keratin, type I cytoskeletal 14 | / | / | / | 5 | 4 | 8 |

[a] Number of peptides identified with ≥99% confidence. [b] Control immunoprecipitations performed using rabbit polyclonal anti-HSP70 antibodies, rabbit IgG or Dynabeads without any immunoglobin attached to them. [c] HSPA2, HSPA1L and HSPA1A are all isoforms of HSP70. [d] Identified peptides also correspond to P01857 - IGHG1 - Immunoglobulin heavy constant gamma 1. [e] Identified peptides for both proteins correspond to P14555 - PLA2G2A - Phospholipase A2, membrane associated. [f] Identified peptides also correspond to P63261 - ACTG1 - Actin, cytoplasmic 2. [g] The identified peptides may result from the autolytic activity of trypsin used during trypsinolysis. /: no peptides identified for the protein.

Supplementary table 3: Summary of the search for hCRISP2 in human sperm proteomes targeting specific post-translational modifications (PTM).

| Targeted PTM | Peptide number | Identified PTM | Reference |
|---|---|---|---|
| **Phosphorylation** | | | (Ficarro et al. 2003) |
| | | | (Parte et al. 2012) |
| | | | (Wang et al. 2015) |
| | | | (Castillo et al. 2019) |
| | 15 | PSer (S52; S56; S212; S216) | (Urizar-Arenaza et al. 2019) |
| | | | (Martin-Hidalgo et al. 2020) |
| | 1 | PSer (S83) | (Wang et al. 2021) |
| **Nitrosylation** | | | (Lefievre et al. 2007) |
| **Glycosylation** | | | (Wang et al. 2013) |
| | | | (Sun et al. 2016) |
| | | | (Xin et al. 2022) |
| **Sumoylation** | | | (Vigodner et al. 2013) |
| **Acetylation** | | | (Wang et al. 2016) |

The shaded areas indicate the proteomes where hCRISP2 was not identified.

## Supplementary references


Anklesaria, J. H., Kulkarni, B. J., Pathak, B. R., and Mahale, S. D. 2016. 'Identification of CRISP2 from human sperm as PSP94-binding protein and generation of CRISP2-specific anti-peptide antibodies', *J Pept Sci*, 22: 383-90.

Busso, D., Cohen, D. J., Hayashi, M., Kasahara, M., and Cuasnicu, P. S. 2005. 'Human testicular protein TPX1/CRISP-2: localization in spermatozoa, fate after capacitation and relevance for gamete interaction', *Mol Hum Reprod*, 11: 299-305.

Busso, D., Goldweic, N. M., Hayashi, M., Kasahara, M., and Cuasnicu, P. S. 2007. 'Evidence for the involvement of testicular protein CRISP2 in mouse sperm-egg fusion', *Biol Reprod*, 76: 701-8.

Castillo, J., Knol, J. C., Korver, C. M., Piersma, S. R., Pham, T. V., De Goeij-De Haas, R. R., Van Pelt, A. M. M., Jimenez, C. R., and Jansen, B. J. H. 2019. 'Human testis phosphoproteome reveals kinases as potential targets in spermatogenesis and testicular cancer', *Molecular and Cellular Proteomics*, 18: S132-S44.

Du, Y., Huang, X., Li, J., Hu, Y., Zhou, Z., and Sha, J. 2006. 'Human testis specific protein 1 expression in human spermatogenesis and involvement in the pathogenesis of male infertility', *Fertil Steril*, 85: 1852-4.

Ficarro, S., Chertihin, O., Westbrook, V. A., White, F., Jayes, F., Kalab, P., Marto, J. A., Shabanowitz, J., Herr, J. C., Hunt, D. F., and Visconti, P. E. 2003. 'Phosphoproteome analysis of capacitated human sperm: Evidence of tyrosine phosphorylation of a kinase-anchoring protein 3 and valosin-containing protein/p97 during capacitation', *Journal of Biological Chemistry*, 278: 11579-89.

Gao, F., Wang, P., Wang, K., Fan, Y., Chen, Y., Chen, Y., Ye, C., Feng, M., Li, L., Zhang, S., and Wei, H. 2021. 'Investigation Into the Relationship Between Sperm Cysteine-Rich Secretory Protein 2 (CRISP2) and Sperm Fertilizing Ability and Fertility of Boars', *Front Vet Sci*, 8: 653413.

Gibbs, G. M., Bianco, D. M., Jamsai, D., Herlihy, A., Ristevski, S., Aitken, R. J., Kretser, D. M., and O'bryan, M. K. 2007. 'Cysteine-rich secretory protein 2 binds to mitogen-activated protein kinase kinase kinase 11 in mouse sperm', *Biol Reprod*, 77: 108-14.

Hardy, D. M., Huang, T. T., Jr., Driscoll, W. J., Tung, K. K., and Wild, G. C. 1988. 'Purification and characterization of the primary acrosomal autoantigen of guinea pig epididymal spermatozoa', *Biol Reprod*, 38: 423-37.

Jamsai, D., Bianco, D. M., Smith, S. J., Merriner, D. J., Ly-Huynh, J. D., Herlihy, A., Niranjan, B., Gibbs, G. M., and O'bryan, M. K. 2008a. 'Characterization of gametogenetin 1 (GGN1) and its potential role in male fertility through the interaction with the ion channel regulator, cysteine-rich secretory protein 2 (CRISP2) in the sperm tail', *Reproduction*, 135: 751-9.

Jamsai, D., Reilly, A., Smith, S. J., Gibbs, G. M., Baker, H. W., Mclachlan, R. I., De Kretser, D. M., and O'bryan, M. K. 2008b. 'Polymorphisms in the human cysteine-rich secretory protein 2 (CRISP2) gene in Australian men', *Hum Reprod*, 23: 2151-9.

Jamsai, D., Rijal, S., Bianco, D. M., O'connor, A. E., Merriner, D. J., Smith, S. J., Gibbs, G. M., and O'bryan, M. K. 2009. 'A novel protein, sperm head and tail associated protein (SHTAP), interacts with cysteine-rich secretory protein 2 (CRISP2) during spermatogenesis in the mouse', *Biol Cell*, 102: 93-106.

Kim, K. S., Foster, J. A., and Gerton, G. L. 2001. 'Differential release of guinea pig sperm acrosomal components during exocytosis', *Biol Reprod*, 64: 148-56.

Lefievre, L., Chen, Y., Conner, S. J., Scott, J. L., Publicover, S. J., Ford, W. C., and Barratt, C. L. 2007. 'Human spermatozoa contain multiple targets for protein S-nitrosylation: an alternative mechanism of the modulation of sperm function by nitric oxide?', *Proteomics*, 7: 3066-84.

Maeda, T., Nishida, J., and Nakanishi, Y. 1999. 'Expression pattern, subcellular localization and structure--function relationship of rat Tpx-1, a spermatogenic cell adhesion molecule responsible for association with Sertoli cells', *Dev Growth Differ*, 41: 715-22.

Maeda, T., Sakashita, M., Ohba, Y., and Nakanishi, Y. 1998. 'Molecular cloning of the rat Tpx-1 responsible for the interaction between spermatogenic and Sertoli cells', *Biochem Biophys Res Commun*, 248: 140-6.

Martin-Hidalgo, D., Serrano, R., Zaragoza, C., Garcia-Marin, L. J., and Bragado, M. J. 2020. 'Human sperm phosphoproteome reveals differential phosphoprotein signatures that regulate human sperm motility', *J Proteomics*, 215: 103654.

Munoz, M. W., Ernesto, J. I., Bluguermann, C., Busso, D., Battistone, M. A., Cohen, D. J., and Cuasnicu, P. S. 2012. 'Evaluation of testicular sperm CRISP2 as a potential target for contraception', *J Androl*, 33: 1360-70.

Nimlamool, W., Bean, B. S., and Lowe-Krentz, L. J. 2013. 'Human sperm CRISP2 is released from the acrosome during the acrosome reaction and re-associates at the equatorial segment', *Mol Reprod Dev*, 80: 488-502.

O'bryan, M. K., Sebire, K., Meinhardt, A., Edgar, K., Keah, H. H., Hearn, M. T., and De Kretser, D. M. 2001. 'Tpx-1 is a component of the outer dense fibers and acrosome of rat spermatozoa', *Mol Reprod Dev*, 58: 116-25.

Parte, P. P., Rao, P., Redij, S., Lobo, V., D'souza, S. J., Gajbhiye, R., and Kulkarni, V. 2012. 'Sperm phosphoproteome profiling by ultra performance liquid chromatography followed by data independent analysis (LC-MSE) reveals altered proteomic signatures in asthenozoospermia', *Journal of Proteomics*, 75: 5861-71.

Sun, Y., Cheng, L., Gu, Y., Xin, A., Wu, B., Zhou, S., Guo, S., Liu, Y., Diao, H., Shi, H., Wang, G., and Tao, S. C. 2016. 'A Human Lectin Microarray for Sperm Surface Glycosylation Analysis', *Mol Cell Proteomics*, 15: 2839-51.

Urizar-Arenaza, I., Osinalde, N., Akimov, V., Puglia, M., Candenas, L., Pinto, F. M., Muñoa-Hoyos, I., Gianzo, M., Matorras, R., Irazusta, J., Blagoev, B., Subiran, N., et al. 2019. 'Phosphoproteomic and functional analyses reveal sperm-specific protein changes downstream of kappa opioid receptor in human spermatozoa', *Molecular and Cellular Proteomics*, 18: S118-S31.

Vigodner, M., Shrivastava, V., Gutstein, L. E., Schneider, J., Nieves, E., Goldstein, M., Feliciano, M., and Callaway, M. 2013. 'Localization and identification of sumoylated proteins in human sperm: Excessive sumoylation is a marker of defective spermatozoa', *Human Reproduction*, 28: 210-23.

Wang, G., Wu, Y., Zhou, T., Guo, Y., Zheng, B., Wang, J., Bi, Y., Liu, F., Zhou, Z., Guo, X., and Sha, J. 2013. 'Mapping of the N-linked glycoproteome of human spermatozoa', *Journal of Proteome Research*, 12: 5750-59.

Wang, J., Qi, L., Huang, S., Zhou, T., Guo, Y., Wang, G., Guo, X., Zhou, Z., and Sha, J. 2015. 'Quantitative phosphoproteomics analysis reveals a key role of Insulin Growth Factor 1 Receptor (IGF1R) tyrosine kinase in human sperm capacitation', *Molecular and Cellular Proteomics*, 14: 1104-12.

Wang, J., Wang, J., Wang, M., Hong, R., Tang, S., Xu, Y., Zhao, X., Zhou, T., Wang, Z., and Huang, S. 2021. 'Quantitative phosphoproteomics reveals GSK3A substrate network is involved in the cryodamage of sperm motility', *Biosci Rep*, 41.

Wang, Y., Wan, J., Ling, X., Liu, M., and Zhou, T. 2016. 'The human sperm proteome 2.0: An integrated resource for studying sperm functions at the level of posttranslational modification', *Proteomics*, 16: 2597-601.

Wittayarat, M., Kiatsomboon, S., Kupthammasan, N., Tipkantha, W., Yimprasert, S., Thongphakdee, A., and Panyaboriban, S. 2024. 'Detection of Protein Biomarkers Relevant to Sperm Characteristics and Fertility in Semen in Three Wild Felidae: The Flat-Headed Cat (Prionailurus planiceps), Fishing Cat (Prionailurus viverrinus), and Asiatic Golden Cat (Catopuma temminckii)', *Animals (Basel)*, 14.

Wittayarat, M., Pukazhenthi, B. S., Tipkantha, W., Techakumphu, M., Srisuwatanasagul, S., and Panyaboriban, S. 2021. 'CRISP protein expression in semen of the endangered Malayan tapir (Tapirus indicus)', *Theriogenology*, 172: 106-15.

Xin, M., You, S., Xu, Y., Shi, W., Zhu, B., Shen, J., Wu, J., Li, C., Chen, Z., Su, Y., Shi, J., and Sun, S. 2022. 'Precision Glycoproteomics Reveals Distinctive N-Glycosylation in Human Spermatozoa', *Mol Cell Proteomics*, 21: 100214.

Zhang, M., Bromfield, E. G., Helms, J. B., and Gadella, B. M. 2022. 'The fate of porcine sperm CRISP2 from the perinuclear theca before and after in vitro fertilization', *Biol Reprod*, 107: 1242-53.

Zhang, M., Bromfield, E. G., Veenendaal, T., Klumperman, J., Helms, J. B., and Gadella, B. M. 2021. 'Characterization of different oligomeric forms of CRISP2 in the perinuclear theca versus the fibrous tail structures of boar spermatozoa', *Biol Reprod*, 105: 1160-70.